

Research and Development of High—Performance Light—Weight Fuel Cell Electrodes

THIRD QUARTERLY REPORT

MAY 1 - JULY 31, 1964

by

R. G. Haldeman, Principal Investigator

W. P. Colman

D. Gershberg

J. D. Ward

prepared for

NATIONAL AERONAUTICS AND SPACE ADMINISTRATION

CONTRACT NAS 3-2786

AMERICAN CYANAMID COMPANY

CYANAMID

NOTICE

This report was prepared as an account of Government-sponsored work. Neither the United States, nor the National Aeronautics and Space Administration (NASA), nor any person acting on behalf of NASA:

- (A) Makes any warranty or representation, expressed or implied, with respect to the accuracy, completeness, or usefulness of the information contained in this report, or that the use of any information, apparatus, method, or process disclosed in this report may not infringe privately owned rights; or
- (B) Assumes any liabilities with respect to the use of or for damages resulting from the use of any information, apparatus, method or process disclosed in this report.

As used above, "person acting on behalf of NASA" includes any employee or contractor of NASA, or employee of such contractor, to the extent that such employee or contractor of NASA, or employee of such contractor prepares, disseminates, or provides access to, any information pursuant to his employment or contract with NASA, or his employment with such contractor.

Requests for copies of this report should be referred to

National Aeronautics and Space Administration
Office of Scientific and Technical Information
Attention: AFSS-A
Washington, D. C. 20546

PLEASE FILE COPY

THIRD QUARTERLY REPORT

RESEARCH AND DEVELOPMENT OF HIGH-PERFORMANCE
LIGHT-WEIGHT FUEL CELL ELECTRODES

by

R. G. Haldeman, Principal Investigator

W. P. Colman

D. Gershberg

J. D. Ward

prepared for

NATIONAL AERONAUTICS AND SPACE ADMINISTRATION

September 15, 1964

CONTRACT NAS 3-2786

Period Covered: May 1, 1964 - July 31, 1964

NASA Lewis Research Center

Cleveland, Ohio

Space Power Systems Division

Technical Manager: Mr. W. A. Robertson MS-86-1

AMERICAN CYANAMID COMPANY

STAMFORD RESEARCH LABORATORIES

1937 West Main Street

Stamford, Connecticut

(Area Code 203) 348-7331

ABSTRACT

The overall object of this contract is the reduction of the weight-to-power ratio of the hydrogen-oxygen fuel cell. Work in the third quarter of the contract has been concentrated on exploration of the operating range of cells made up with Standard and High-Loading electrodes in combination with Fuel Cell and ACCO Asbestos matrices. Extensive life-testing was also conducted and factors contributing to performance decline investigated.

A 6 inch x 6 inch active area test cell was designed and constructed. Theoretical analysis was made of the electrolyte concentration and temperature gradients to be expected in a fuel cell operating with dynamic heat and water removal with no auxiliary cooling.

TABLE OF CONTENTS

	<u>Page</u>
1. <u>INTRODUCTION</u>	1
1.1 Objectives	1
1.2 Scope	1
2. <u>SUMMARY</u>	2
3. <u>MATERIALS INVESTIGATIONS</u>	6
3.1 Microscopic Examination of Used Fuel Cell Electrodes	6
3.2 Corrosion Tests	11
4. <u>ELECTRODE DEVELOPMENT</u>	13
5. <u>SMALL SCALE TESTING</u>	14
5.1 Performance vs. Operating Conditions	14
5.1.1 Matrix Thickness	14
5.1.2 Cell Assembly Pressure and Electrolyte Loading	20
5.1.3 Electrolyte Concentration	23
5.1.4 Pressure	33
5.1.5 Temperature	33
5.1.6 High Temperature and Electrolyte Concentrations	40
5.1.7 Electrode and Matrix Type	40
5.1.8 Carbonate Concentration	42
5.2 Life-Testing	44
5.2.1 Used Electrodes	44
5.2.2 High-Loading Electrodes	44
5.2.3 Matrix Variations	47
5.2.4 Tests at 100°C	48

TABLE OF CONTENTS

(Continued)

	<u>Page</u>
5.2.5 High Current Densities	50
5.2.6 Effect of Gas Reversals	51
5.2.7 Variations in Waterproofing Level	51
5.2.8 Platinum and Teflon Screens	52
5.2.9 Cell Design for Life-Testing	56
6. <u>SCALE-UP</u>	58
6.1 Choice of Operating Conditions	58
6.2 Design of 6" x 6" Cell	61
6.3 Mathematical Simulation of Fuel Cell Operation	63
6.3.1 Development of the Model	64
6.3.1.1 Physical Picture and Assumptions	64
6.3.1.2 Derivation of the Performance Equations	68
6.3.2 Solution for the Dynamic System with No Auxiliary Cooling	79
6.3.2.1 Linear Solution	79
6.3.2.2 Analog Solution	83
6.3.3 Application to Dynamic System with No Auxiliary Cooling	83
6.3.4 Summary - Dynamic System with No Auxiliary Cooling	91
7. <u>FUTURE WORK</u>	93
<u>Appendix A</u> - Nomenclature for Mathematical Analysis	94
<u>Appendix B</u> - Effect of Transfer Coefficients	96
<u>References</u>	98
Distribution List for Third Quarterly Report	99

LIST OF TABLES

<u>Tables</u>	<u>Titles</u>	<u>Page</u>
3-1	Metals for Corrosion Testing	11
5-1	Distribution of Electrolyte After Cell Assembly	19
5-2	Effect of Pressure on Cell Performance	34
5-3	Cell Performance vs. Temperature	39
5-4	Cell Performance at High Temperatures and Concentrations	41
5-5	Effect of Carbonate Concentration on Cell Performance	43
5-6	Life Test Summary	45
5-7	Life Test of Used Electrodes	46
6-1	Operating Conditions for Scale-up	59
6-2	Concentration Gradients as a Function of Inlet Flow Conditions	86

LIST OF FIGURES

<u>Figures</u>	<u>Titles</u>	<u>Page</u>
3-1	Electron Micrograph: Extraction Replica of Surface of Unused AB-1 Electrode	8
3-2	Electron Micrograph: Extraction Replica of Front (Matrix Side) Surface of Used AB-1 Oxygen Electrode	9
3-3	Electron Micrograph: Extraction Replica of Front (Matrix Side) Surface of Used AB-1 Hydrogen Electrode	10
5-1	Voltage vs. Matrix Thickness: ACCO Asbestos	15
5-2	Voltage vs. Matrix Thickness: Fuel Cell Asbestos	16
5-3	Cell Internal Resistance vs. Matrix Thickness	18
5-4	Cell Internal Resistance vs. Electrolyte Loading and Assembly Pressure	22
5-5	Cell Performance vs. Electrolyte Loading and Assembly Pressure: ACCO Asbestos, AB-1 Electrodes	24
5-6	Cell Performance vs. Electrolyte Loading: ACCO Asbestos, High-Loading Electrodes	25
5-7	Cell Internal Resistance v . KOH Concentration	26
5-8	Cell Performance vs. KOH Concentration: AB-1 Electrodes, Fuel Cell Asbestos	28
5-9	Cell Performance vs. KOH Concentration: AB-1 Electrodes, ACCO Asbestos	29
5-10	Cell Performance vs. KOH Concentration: High-Loading Electrodes, Fuel Cell Asbestos	30
5-11	Cell Performance vs. KOH Concentration: High-Loading Electrodes, ACCO Asbestos	31
5-12	Cell Internal Resistance vs. Temperature	35
5-13	Cell Performance vs. Temperature: 5N KOH	37

LIST OF FIGURES

(Continued)

<u>Figures</u>	<u>Titles</u>	<u>Page</u>
5-14	Cell Performance vs. Temperature: 13N KOH	38
5-15	Life Test 2-33 at 100°C	49
5-16	Life Test 2-39: Platinum on Platinum Screen Electrodes	53
5-17	Polarization Data: Platinum on Teflon Screen Electrodes	55
5-18	2" x 2" Pressure Cell	57
6-1	6" x 6" Cell Design	62
6-2	Cell Configuration for Mathematical Model	65
6-3	Vapor Pressure Data Correlation	82
6-4	Analog Simulation of Hydrogen-Oxygen Fuel Cell	84
6-5	Preliminary Flow Sheet - Dynamic System with No Auxiliary Cooling	85
6-6	Typical Normality Profile - Dynamic System with No Auxiliary Cooling	90

1. INTRODUCTION

1.1 Objectives

The objectives of the National Aeronautics and Space Administration Contract NAS 3-2786 are indicated by Article I in the Statement of Work of RFP No. APGO-1508.

ARTICLE I - OBJECTIVES

(a) A fuel cell utilizing hydrogen and oxygen reactants is of considerable interest to NASA because of its high electrical work output per unit of weight of reactants. The efficiency of hydrogen-oxygen fuel cells is 60% or better in practical cells. These cells have a power plant weight of approximately 150 pounds per kilowatt neglecting reactants and tankage. The chief objective of hydrogen-oxygen fuel cell research is the reduction of the weight-to-power ratio.

(b) An important factor in determining the fuel cell weight is the weight of the electrode and its supporting structure. The intent is to support research and development efforts directed towards obtaining electrode systems which will produce a higher electrochemical reaction rate per unit weight of electrode and assembly while maintaining a satisfactory fuel consumption efficiency.

(c) While this RFP suggests that high-performance, light-weight electrodes are the basic interest, it should be understood that the weight and efficiency of the entire power plant must be included to in fact achieve the purpose of this effort: namely, the reduction of the fuel cell weight-to-power ratio.

1.2 Scope

The scope of work to be done by American Cyanamid Company during the contract year is outlined in the Schedule of Work, presented in the First Quarterly Report (1).

Work in the third quarter under Phase I of the Schedule of Work was devoted primarily to the evaluation of performance of several promising electrode-matrix combinations over a wide range of experimental conditions. Extensive life testing was conducted. In addition, work under Phase II of the Schedule of Work was undertaken to scale up to 6 inch x 6 inch single cells, and to consider analytically the design of a gas distributor plate to be used in a prototype battery stack. Plans for work in the fourth quarter of this contract are included in the last section of this report.

2. SUMMARY

Following is a summary of the major findings of the third quarterly report period.

(1) Microscopic examinations indicate possible sintering of platinum on the hydrogen electrode surface facing the asbestos matrix during extended tests. There is no evidence that this change has any effect on electrode performance.

(2) A study was made over a wide range of operating conditions of the performance characteristics of cells having components consisting of the four possible combinations of Standard and High-Loading electrodes, with Fuel Cell Asbestos, and ACCO Asbestos.

(3) Optimum matrix thickness appears to be 20-40 mils for ACCO Asbestos and 10-20 mils for Fuel Cell Asbestos. Use of this thickness permits maximum stable current densities of over 1000 ma/cm² in short term tests.

(4) Minimum cell resistance and maximum cell performance was achieved at cell assembly pressure in the range 60-180 psi and at electrolyte loadings of 1.5-3.0 g electrolyte/g ACCO Asbestos or 0.5-1.0 g/g of Fuel Cell Asbestos.

(5) In general, cell performance increased with increasing concentration of electrolyte at all current densities except at or very close to maximum stable current densities. Performance decreased sharply at concentrations below 3-5N, probably because the high partial pressure of water interferes with transport of reactants.

(6) Increase of absolute pressure to two atmospheres markedly improved performance at low electrolyte concentrations. Thus, an increase in potential of 130 millivolts at 200 ma/cm² is observed at 100°C in 3N KOH. Maximum stable current density is increased from 200 to 1200 ma/cm² by the same increase in pressure.

(7) Performance generally increased and cell internal resistance generally decreased as temperature was increased in the range 70-100°C. The temperature effect was more pronounced at higher electrolyte concentrations. Performance at high current densities (e.g., 1000 ma/cm²) is generally more stable when the cells are operated at higher temperatures.

(8) The operating temperature range was extended to 140°C and electrolyte concentration to 15-19N. Using High-Loading electrodes and ACCO Asbestos, the combination of higher temperature and electrolyte concentration permits a further improvement in performance. Thus, highest performance was achieved at 140°C with 19N KOH. Working potential was 0.99 volt at 200 ma/cm² and 0.84 at 600 ma/cm².

(9) The combination of High-Loading electrodes and ACCO Asbestos proved best from the standpoint of achieving maximum performance in short term tests. Life-testing is in progress to determine the comparative long term stability of these systems.

(10) In a study of the effect of carbonate concentration on performance it appears that over the range 0-200 ma/cm² performance is governed by absolute KOH concentration and is affected little by addition of carbonate up to an equal concentration by weight.

(11) Life tests with High-Loading electrodes showed, in general, a higher level of performance than with Standard electrodes. Magnitude of voltage decline with time was about the same as for Standard electrodes. High-Loading electrodes perform more stably at higher current densities.

(12) A cell containing Standard AB-1 electrodes was operated at 100 ma/cm² at 100°C for 1105 hours. Average decline rate was about 3 mv/100 hours.

(13) A cell containing Standard AB-1 electrodes has been operated for 337¹/₄ hours at 100 ma/cm² at 70°C. During this period gases were reversed (hydrogen on the oxygen side and vice versa) four times and cell potential was maintained between 0.835 and 0.81 volt.

(14) Tests were run in which nickel parts of the fuel cell were systematically replaced by platinum. It appears that the small observed decline in cell performance can be attributed to formation of an oxide on the cathode support screen. Means of overcoming this problem are under investigation.

(15) A pressure cell was constructed and tested satisfactorily at pressures up to 60 psig.

(16) Optimum operating conditions for scale-up were chosen depending on whether or not fuel and associated tankage is included in total weight. In the former case operation at 13N KOH is preferred, in the latter case 5N KOH is preferred. The choice depends on the relative importance of weight and power requirements of the hydrogen circulation pump.

(17) A 6 inch x 6 inch single cell employing a gas distribution system proven satisfactory by tests on a plastic model was designed and constructed.

(18) In order to study theoretically the performance of a given cell in a battery stack as it will be influenced by gradients in electrolyte concentration, electrolyte loading, and temperature, a mathematical model has been developed. General differential mass and energy balances were set up and solved for a system employing dynamic heat and water removal from the battery with no auxiliary cooling. Similar calculations are in progress for the case with auxiliary cooling.

- (19) This simulation predicts for dynamic heat and water removal:
- a. Temperature and partial pressure of water in the bulk hydrogen stream will be essentially the same as at the adjacent electrode surface at any point, even at current densities in excess of 500 ma/cm^2 .
 - b. The steady state electrolyte concentration gradients will depend only on the temperature gradients.
 - c. Overall temperature and electrolyte concentration gradients should be independent of the distance between the inlet and outlet channels.
 - d. Preheating of the hydrogen stream entering the battery will be necessary to maintain KOH concentration above $5N$.
 - e. In order to limit concentration gradients to a $2-3N$ variation internal cooling will be required.

3. MATERIALS INVESTIGATION

3.1 Microscopic Examination of Used Fuel Cell Electrodes

During the course of the life-testing program, it has been observed that the hydrogen electrode almost invariably develops a rather uniform grey discoloration on the side facing the matrix. This "greying" is not observed on the gas side of the hydrogen electrode, or on either side of the oxygen electrode. Further, there is a tendency for the hydrogen electrode (but not the oxygen electrode) to stick to the asbestos matrix.

In order to aid in interpretation of these observations, a number of electrodes were submitted for electron microscopy. The electrode surfaces were examined by a gelatin-silica replica technique which, in addition to replicating the surface topography, also enabled a portion of the constituents to be removed from the surface of the electrode for direct examination in the electron microscope.

Samples submitted included unused electrodes, electrodes used in life tests of varying duration, and electrodes exposed to hydrogen or oxygen in a fuel cell assembly but with the same gas on both sides so that there was no electrochemical reaction.

Both surfaces of the used electrodes (i.e. - matrix side and gas side) were examined by electron microscopy. Only on the matrix side of the hydrogen electrodes tested under current drain was there any discernable difference between the used and unused electrodes.

At this surface the platinum particles appeared coarser and more compact than on the other surfaces. This effect is illustrated in Figures 3-1 to 3-3. Figure 3-1, an extraction replica of an unused electrode shows Teflon latex particles and fibrils and aggregates of platinum particles. Figure 3-2 shows a replica of the matrix side of a used oxygen electrode. Note that the "finestructure" of the platinum, visible around the edges of the aggregates, is similar to that in the unused electrode. Figure 3-3 shows the matrix side of a used hydrogen electrode. This surface was visibly greyed. The extraction replica indicates an apparent growth of the ultimate platinum particles and compaction of the aggregates.

The microscopic examinations described above indicate some possible sintering of the platinum on the hydrogen electrode surface. The fact that the changes observed occurred only at the matrix side of the hydrogen electrode, and only when current was being drawn from the cell, suggests that this sintering may be caused by the heat released by neutralization of hydrogen ions as they are formed at the electrode-electrolyte interface.

While there is strong evidence that some sort of sintering process occurs under life test conditions, there is no real indication that this sintering has any appreciable effect on electrode performance. Electrodes which have developed a very pronounced grey surface during life-testing (those from life 2-45, for example) have been shown to retain their original activity.

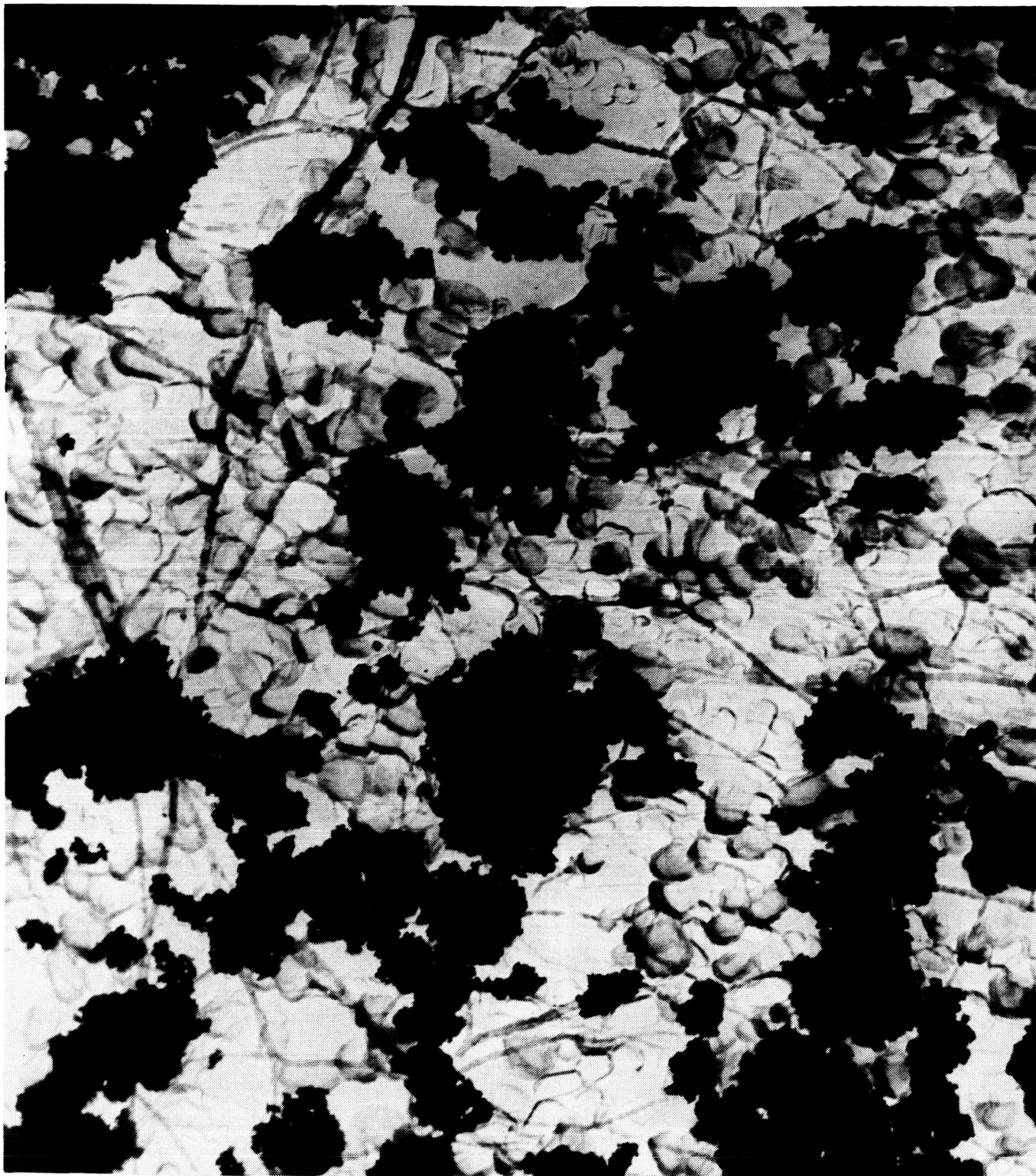


FIGURE 3-1 Extraction Replica of Surface of Unused AB-1 Electrode, 6464-51-15.
EM 20,000X
16393-5

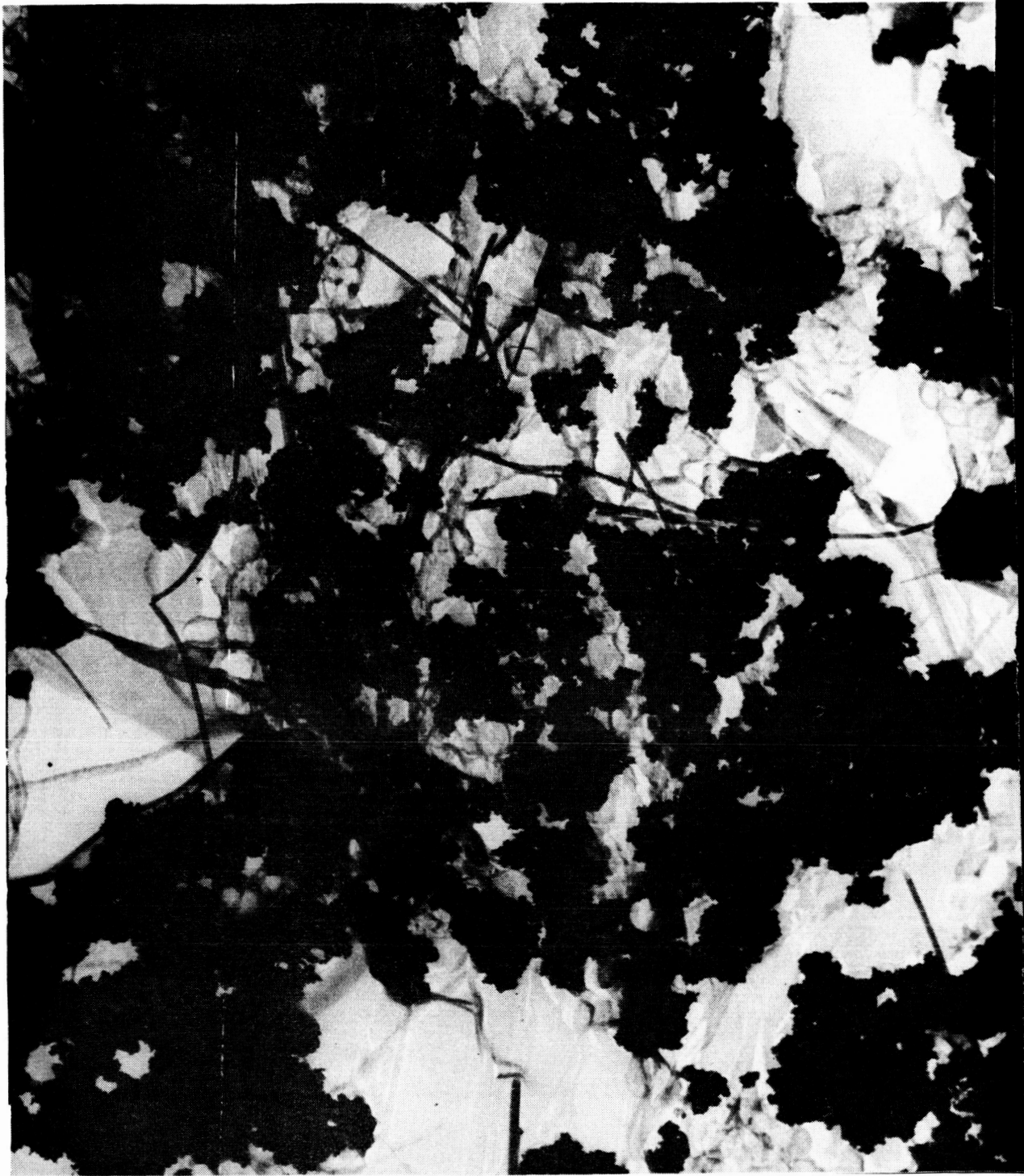


FIGURE 3-2 Extraction Replica of Front (Matrix Side) Surface of Used
AB-1 Oxygen Electrode, EM 20,000X 16397-5



FIGURE 3-3 Extraction Replica of Front (Matrix Side) Surface of Used AB-1 Hydrogen Electrode, EM 20,000X 16397-5

3.2 Corrosion Tests

Oxidation of nickel cell parts is believed to be a factor contributing to the downward performance trends observed in the life-testing program (see section 5.2.8). Several approaches to this problem are being investigated.

- (a) Plating nickel parts (screens) with precious metals.
- (b) Development of conductive oxide films by lithiation or by electrochemical means.
- (c) Substitution of more corrosion-resistant, non-precious metals.

For part (c), corrosion tests have been initiated on twelve metals selected after a survey of the literature. These metals are listed in Table 3-1.

TABLE 3-1
Metals for Corrosion Testing

<u>Alloy</u>	<u>Major Constituents, Wt. %</u>									
	<u>Cr</u>	<u>Ni</u>	<u>Mo</u>	<u>Cu</u>	<u>Fe</u>	<u>Ti</u>	<u>Co</u>	<u>W</u>	<u>Al</u>	<u>Cb</u>
Monel	-	67	-	31	-	-	-	-	-	-
Hastelloy R-235	15	65	5	-	9.5	2.5	-	-	2	-
Hastelloy B	-	66	27	-	5	-	-	-	-	-
Hastelloy C	15	56	16	-	6	-	1	4	-	-
Carpenter 20 Cb	20	27	2.5	3.5	44	-	-	-	-	1
Nimonic 75	20	77	-	-	1	-	-	-	-	-
Incoloy 804	30	44	-	-	24	-	-	-	-	-
Inconel	15	77	-	-	7	-	-	-	-	-
Alloy 25	19	9	-	-	3	-	51	15	-	-
Nickel										
Nickel L (Low Carbon)										
Zirconium										

Corrosion tests on the above metals are in progress. Sample coupons were partially submerged in a 35 wt. % KOH solution at 110°C, with oxygen bubbling through. The samples are to be checked for resistance to tarnishing and for weight loss. It may also be possible to obtain information pertinent to the use of these metals in fuel cells by measuring the electrical resistance of the samples (including surface oxide films) after exposure in the corrosion tests.

While these corrosion tests are still in progress, some qualitative observations can be made at the present time. All of the samples showed some degree of tarnishing within ten days of exposure. The best metals from this standpoint appear to be zirconium, low-carbon nickel, and Inconel.

4. ELECTRODE DEVELOPMENT

For the present, High-Loading electrodes containing 40 mg Pt/cm² and 25% Teflon deposited on a 40 mesh 10 mil wire nickel screen are considered as the new preferred electrode for use in life-testing and scale-up programs. Investigations currently in progress in the areas of life-testing and corrosion resistance should determine if further modifications are desirable.

5. SMALL SCALE TESTING

5.1 Performance vs. Operating Conditions

In order to determine operating conditions which give maximum performance, the investigation was continued on the effect of cell assembly and operating variables for the following four electrode-matrix systems:

<u>Electrodes</u>	<u>Matrix</u>
Standard Type AB-1 (9 mg Pt/cm ²)	ACCO Asbestos ^(a)
Standard Type AB-1 (9 mg Pt/cm ²)	Fuel Cell Asbestos ^(a,b)
High-Loading (40 mg Pt/cm ²)	ACCO Asbestos
High-Loading (40 mg Pt/cm ²)	Fuel Cell Asbestos

Cell assembly and operating variables included:

1. matrix thickness
2. cell assembly pressure
3. electrolyte loading
4. electrolyte concentration
5. temperature
6. pressure

5.1.1 Matrix Thickness

The effect of matrix thickness was studied in 1" cells. At 100°C, using High-Loading electrodes, 13N KOH, and varying numbers of sheets of Fuel Cell or ACCO Asbestos. In the range 20-40 mils^(c) for ACCO Asbestos or 10-20 mils for Fuel Cell Asbestos, the working voltage was essentially independent (within 20 mv) of matrix thickness for current densities up to 300 ma/cm². (See Figures 5-1 and 5-2.)

(a) Described in Reference (1)(First Quarterly Report)

(b) Johns-Manville Co.

(c) In the present discussion thickness prior to compression in the cell is used for comparative purposes.

VOLTAGE VS. MATRIX THICKNESS - ACCO ASBESTOS

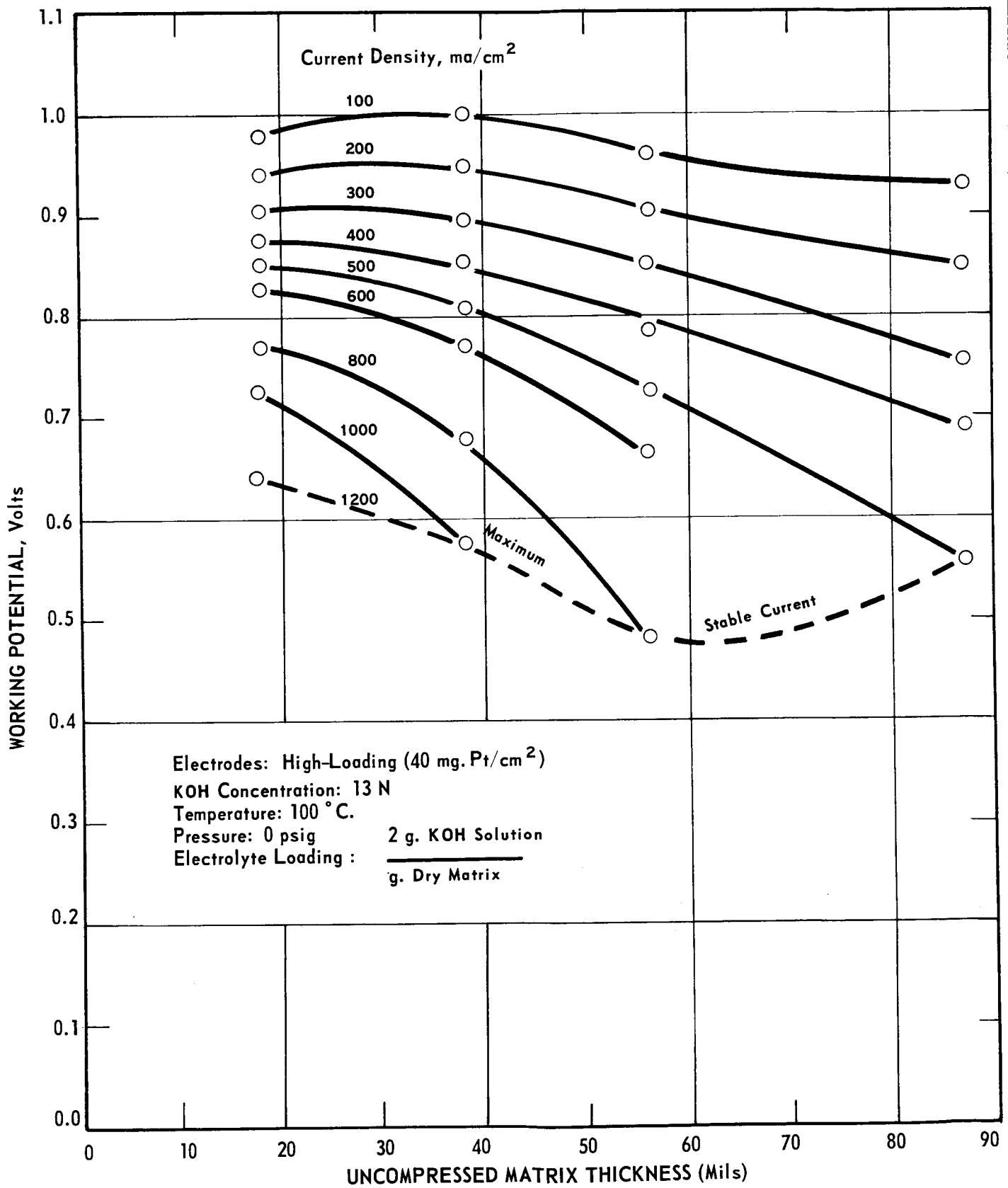


FIGURE 5-1

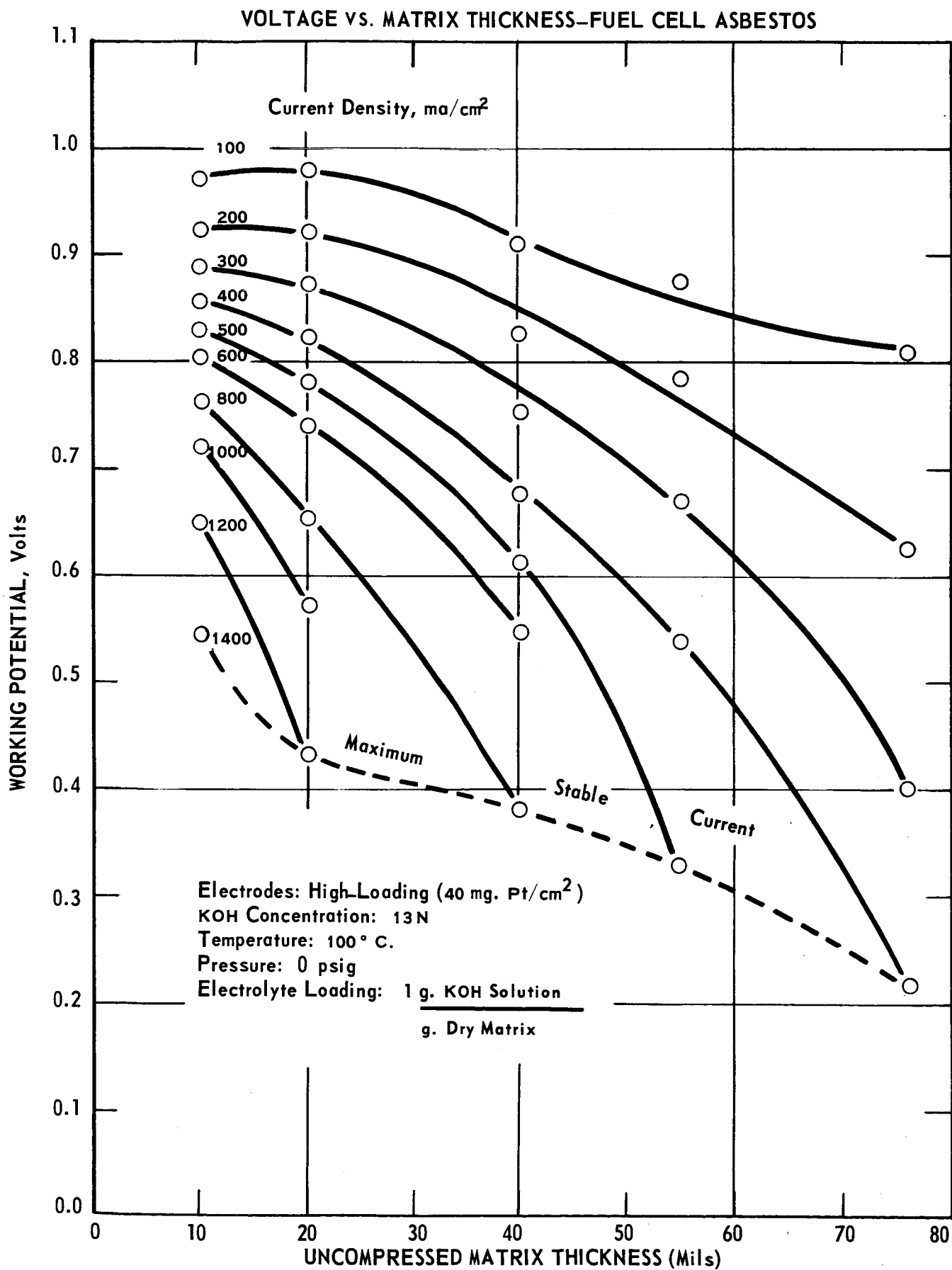


FIGURE 5-2

At greater matrix thicknesses and at higher current densities, cell voltage falls markedly, and a characteristic maximum stable current density^(a) for each thickness and type of asbestos has been determined. This quantity is indicated by the dashed lines in Figures 5-1 and 5-2. These data show that 10-20 mil matrix thickness would be most suitable for maximum performance over a wide range of current densities.

At equal matrix thickness and equal total electrolyte loadings^(b), the two matrix materials yielded comparable voltages for thicknesses up to 20 mils and current densities up to 200 ma/cm². At higher thicknesses and current densities, ACCO Asbestos yielded increasingly higher voltages than Fuel Cell Asbestos. This resulted partly from the lower internal resistance of cells containing the relatively more porous ACCO Asbestos. With either matrix, the increase in cell internal resistance^(c) with increasing matrix thickness accounted for roughly 75-90% of the decrease in voltage in the lower ranges of current density and matrix thickness, and only 25-40% in the upper ranges. The latter data indicate increasing electrolyte diffusion limitations with increasing matrix thickness and current density.

(a) Maximum current density is the approximate limit at which stable operation in a short term test (15 minutes) can be achieved.

(b) At equal thicknesses, 2 g solution/g dry ACCO Asbestos gives the same total electrolyte loading as 1 g solution/g dry Fuel Cell Asbestos, since the former is approximately half as dense as the latter.

(c) Cell internal resistance measured by a Keithley Model 502 milliohmmeter.

CELL INTERNAL RESISTANCE vs. MATRIX THICKNESS

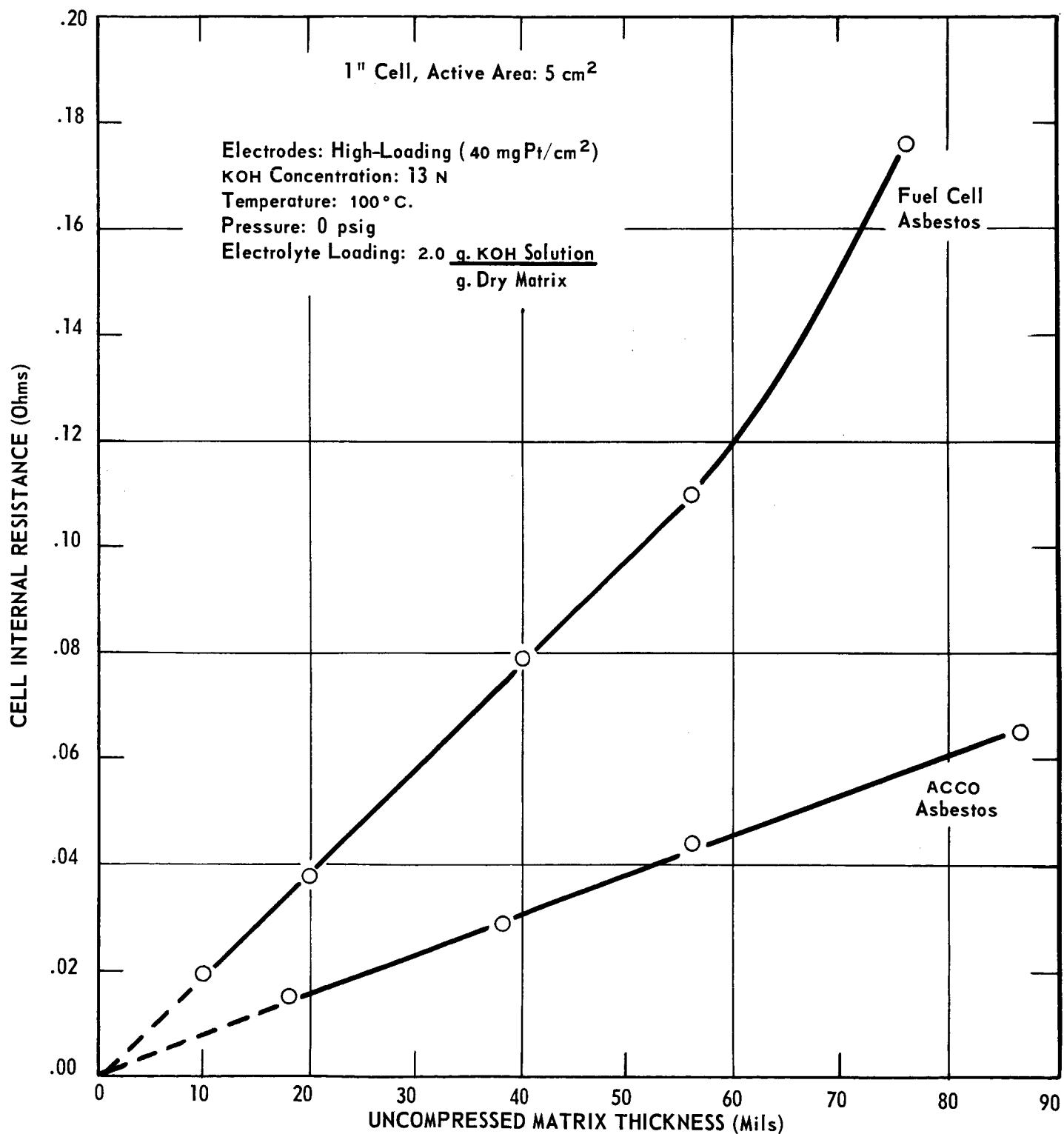


FIGURE 5-3

TABLE 5-1
DISTRIBUTION OF ELECTROLYTE AFTER CELL ASSEMBLY (a)

Initial Electrolyte Loading g/g(b)	Amount of Electrolyte Retained in:				
	Matrix g/g(b)	% (c)	Electrodes g/g (b)	% (c)	Spacer Screens g/g (b) % (c)
0.50	0.333	67	.079	16	.088 17
1.00	0.800	80	.086	9	.114 11
2.00	1.74	87	.104	5	.160 8
3.00	2.64	88	.118	4	.242 8

(a) Standard AB-1 Electrodes 20 Mil ACCO Asbestos. Assembly Pressure 60-180 psi.

(b) Grams Solution / Gram Dry Matrix.

(c) % of Electrolyte Initially Loaded.

As shown in Figure 5-3 cell internal resistance was proportional to matrix thickness and extrapolated to zero resistance at zero thickness, indicating no other significant cell losses. Resistivities were calculated from the slopes of the lines in Figure 5-3. As shown below, that for ACCO Asbestos is lower than that for Fuel Cell Asbestos, and both, as would be expected, are greater than that for the electrolyte alone⁽³⁾.

	Resistivity (ohm-cm)
ACCO Asbestos + 13N KOH at 100°C	1.49
Fuel Cell Asbestos + 13N KOH at 100°C	3.86
13N KOH at 100°C	0.68

5.1.2 Cell Assembly Pressure and Electrolyte Loading

Previous work⁽²⁾ showed the effect of initial electrolyte loading and cell assembly pressure on electrolyte distribution, cell internal resistance and performance with Standard AB-1 electrodes and Fuel Cell Asbestos matrix in 2" x 2" cells. Similar data were obtained this quarter for both Standard AB-1 electrodes and High-Loading electrodes, using ACCO Asbestos and equivalent conditions of matrix thickness (20 mils), temperature (70°C), pressure (atmospheric), and KOH concentration (7M).

For the Standard AB-1 electrode - ACCO Asbestos matrix system, Table 5-1 shows the distribution of electrolyte in the assembled cell among the matrix, the electrodes, and the spacer screens for initial electrolyte loadings ranging from 0.5-3.0 g/g. This distribution was virtually independent of cell assembly pressure from 30-180 psi over the entire range of electrolyte loadings. Comparison^(a) with data reported previously⁽²⁾ for the Standard AB-1 electrodes - Fuel Cell Asbestos matrix system at 60-180 psi indicates the following similarities:

(a) See footnote (b), preceding page

1. The amount of electrolyte remaining in the matrix after assembly was nearly proportional to the electrolyte loading.

2. At a given absolute amount of electrolyte loaded, the percentage pressed out of the matrix (12-33%) was essentially the same for the two matrices.

3. The quantity of electrolyte pressed into the electrodes increased relatively little with loading, was roughly the same for each system, and amounted to about 14-28% of the dry electrode weight (compared to a "saturation" level of about 40%) for the two matrix systems.

The effects of electrolyte loading and cell assembly pressure on cell internal resistance are shown in Figure 5-4. With both AB-1 and High-Loading electrodes, cell resistance was very high at electrolyte loadings of 0.5 g/g, but dropped sharply to a minimum at about 1.5 g/g. Cell assembly pressure in the 60-180 psi range had very little effect on internal resistance. The high cell resistances obtained at low electrolyte loadings may indicate that under these conditions the electrolyte cannot distribute evenly throughout the matrix so that some areas are left dry. For both Standard and High-Loading electrodes, the optimum conditions for low cell internal resistance are at electrolyte loadings of 1.5-3.0 g/g and cell assembly pressures in the range 60-180 psi. Similar optimum conditions with respect to absolute amount of electrolyte and cell assembly pressure were previously found for the system consisting of Standard AB-1 electrodes and Fuel Cell Asbestos Matrix.

CELL INTERNAL RESISTANCE vs. ELECTROLYTE LOADING AND ASSEMBLY PRESSURE

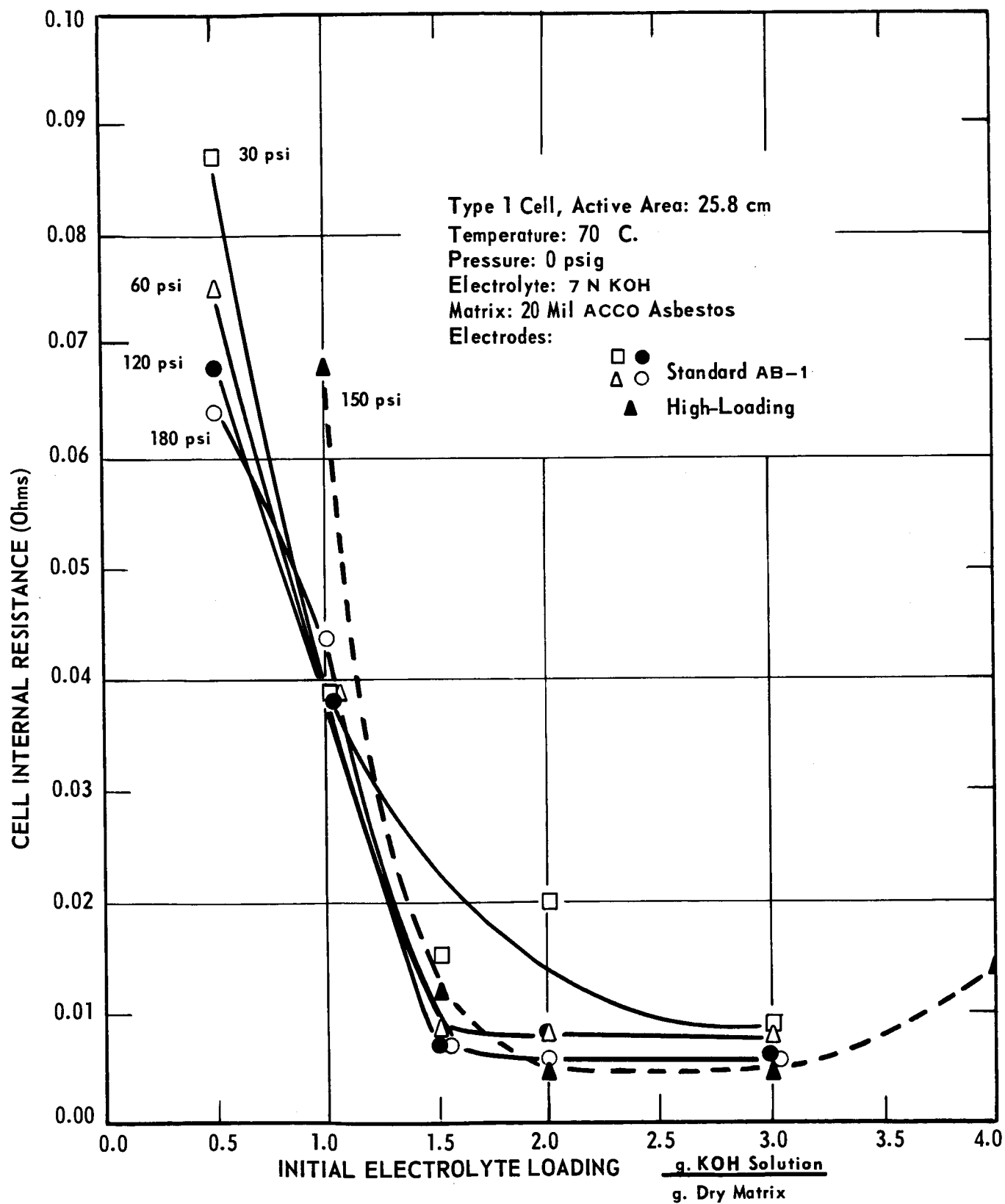


FIGURE 5-4

Figures 5-5 and 5-6 show the effect of electrolyte loading on performance with ACCO Asbestos matrix. In this case, the data were obtained at 70°C, using 7N KOH. Figure 5-5 shows data for Standard AB-1 electrodes and Figure 5-6 data for High-Loading electrodes. Figure 5-5 also shows the effect of cell assembly pressure in the range 60-180 psi.

With either type of electrode, no current could be drawn at loadings of 1.0 g/g, probably because this amount of electrolyte was insufficient to permit good electrolytic contact between matrix and electrodes. At higher loadings, stable current densities of 100-400 ma/cm² were obtained. The cell assembly conditions for optimum performance are 2-3 grams KOH solution per gram dry matrix and an assembly pressure of 120-180 psi, i.e., roughly the same as already noted for minimum cell resistance. As reported previously,⁽²⁾ these same conditions (in terms of absolute electrolyte loading) give optimum performance with the Standard AB-1 electrodes - Fuel Cell Asbestos matrix system. While no data of this type were obtained for the High-Loading electrode - Fuel Cell Asbestos matrix system, it seems reasonable to assume that equivalent conditions are optimum for that system also.

5.1.3 Electrolyte Concentration

Figure 5-7 shows the effect of KOH concentration on the internal resistance in one-inch diameter cells for the four electrode matrix systems at 100°C; similar data at 70°C was reported previously⁽²⁾. The optimum electrolyte loading (1.0 and 2.0 g/g for Fuel Cell Asbestos and ACCO Asbestos, respectively) and cell assembly pressure

CELL PERFORMANCE vs. ELECTROLYTE LOADING AND ASSEMBLY PRESSURE
ACCO ASBESTOS, AB-1 ELECTRODES

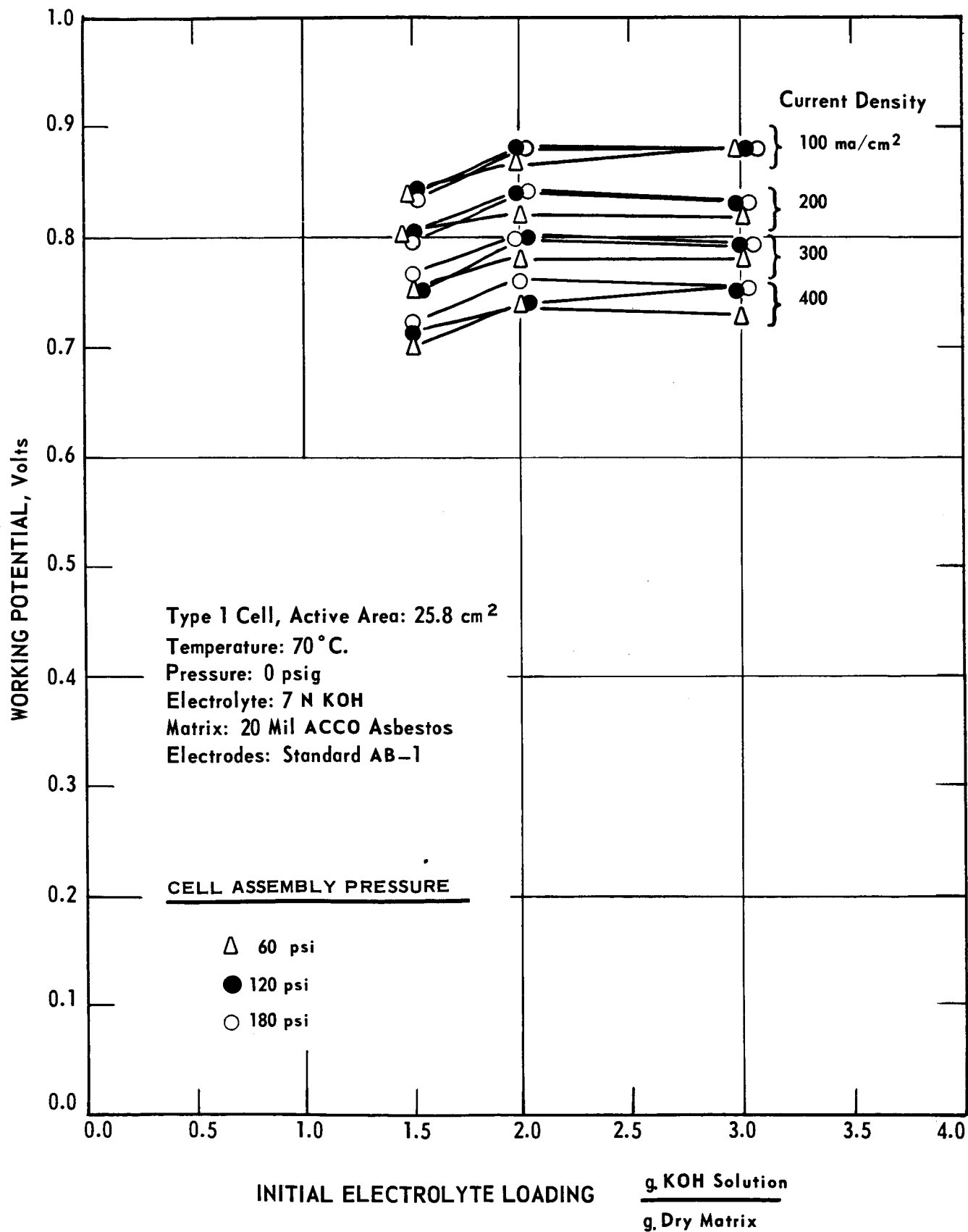


FIGURE 5-5

CELL PERFORMANCE vs. ELECTROLYTE LOADING

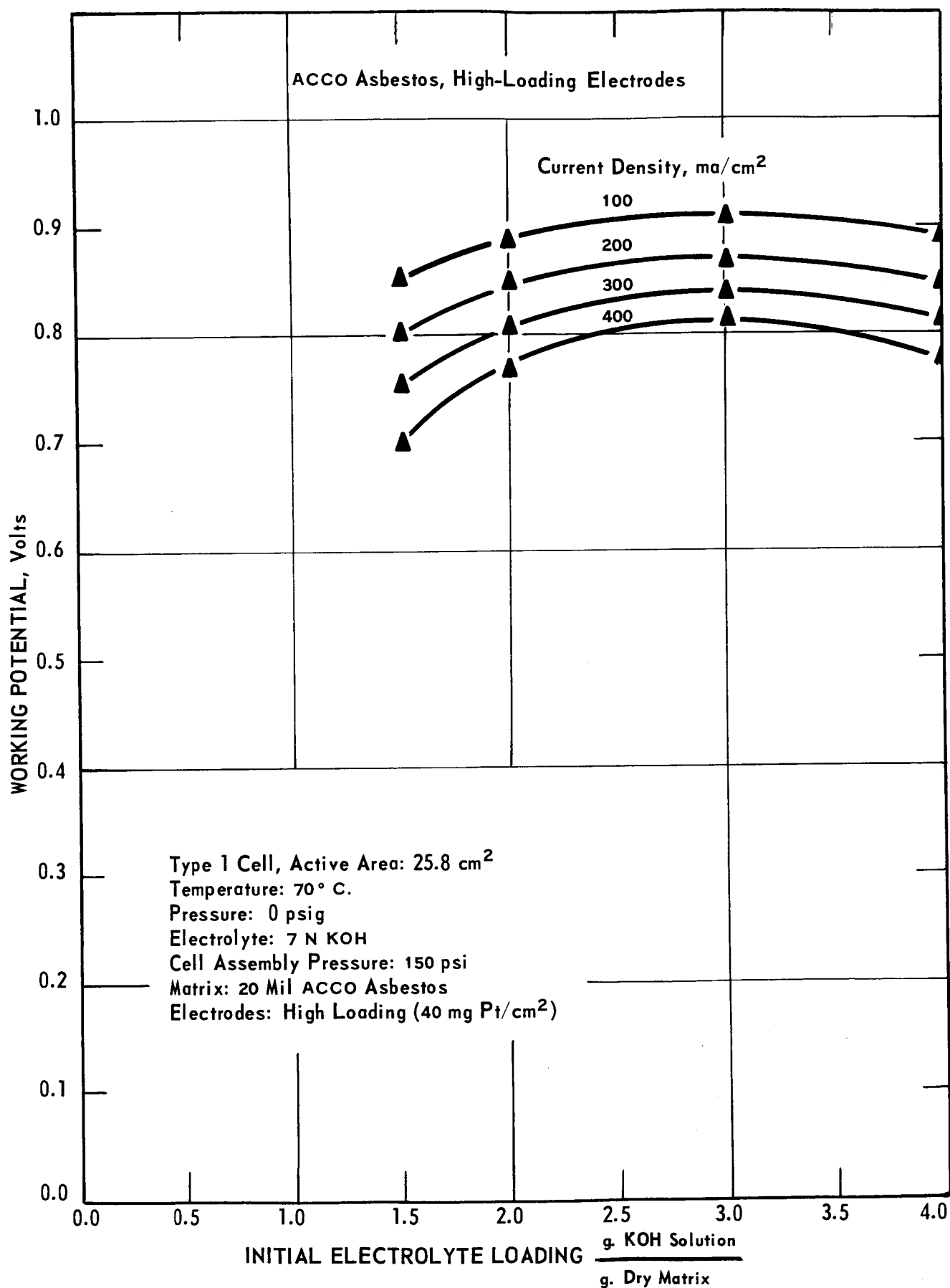


FIGURE 5-6

CELL INTERNAL RESISTANCE vs. KOH CONCENTRATION

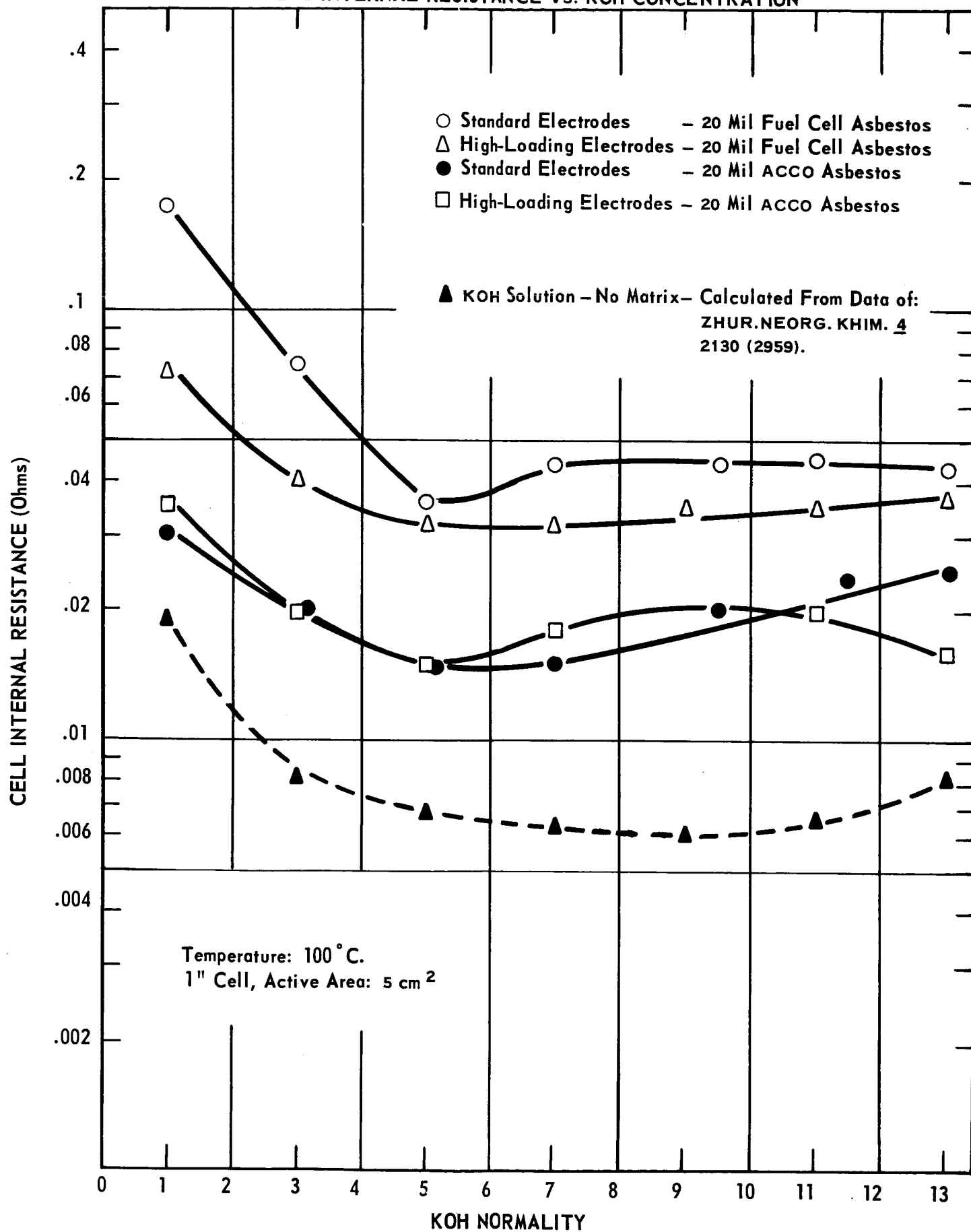


FIGURE 5-7

120-180 psi) were used. The matrix was 20 mils thick. Cell resistance is little affected by electrode type. ACCO Asbestos gave lower resistance than Fuel Cell Asbestos, in combination with either electrode, over the entire range of KOH concentration (1-13N). Resistance decreased sharply with increase in concentration in the range 1-3N and was little affected in the range 3-13N. The resistance - concentration curves have the same general shape as the equivalent curve for free electrolyte. The latter was calculated from published conductivity data for aqueous KOH at 100°C⁽³⁾, using an area equal to the active area of the cell and thickness equal to that of the uncompressed matrix.

The dependence of cell performance on KOH concentration at 100°C and atmospheric pressure is shown in Figures 5-8 through 5-11 for the four electrode-matrix systems. Similar data at 70°C were reported previously⁽²⁾. At each concentration, the highest current density shown is the maximum current density which could be sustained in a short term test. At the highest current densities, there is considerable scatter in the data, leading to considerable uncertainty in the curves shown. Concentration effects at 13-17N with High-Loading electrodes and ACCO Asbestos were investigated by loading 13N KOH into the matrix and then concentrating in the cell with gas flows in excess of those required to maintain 13N KOH.

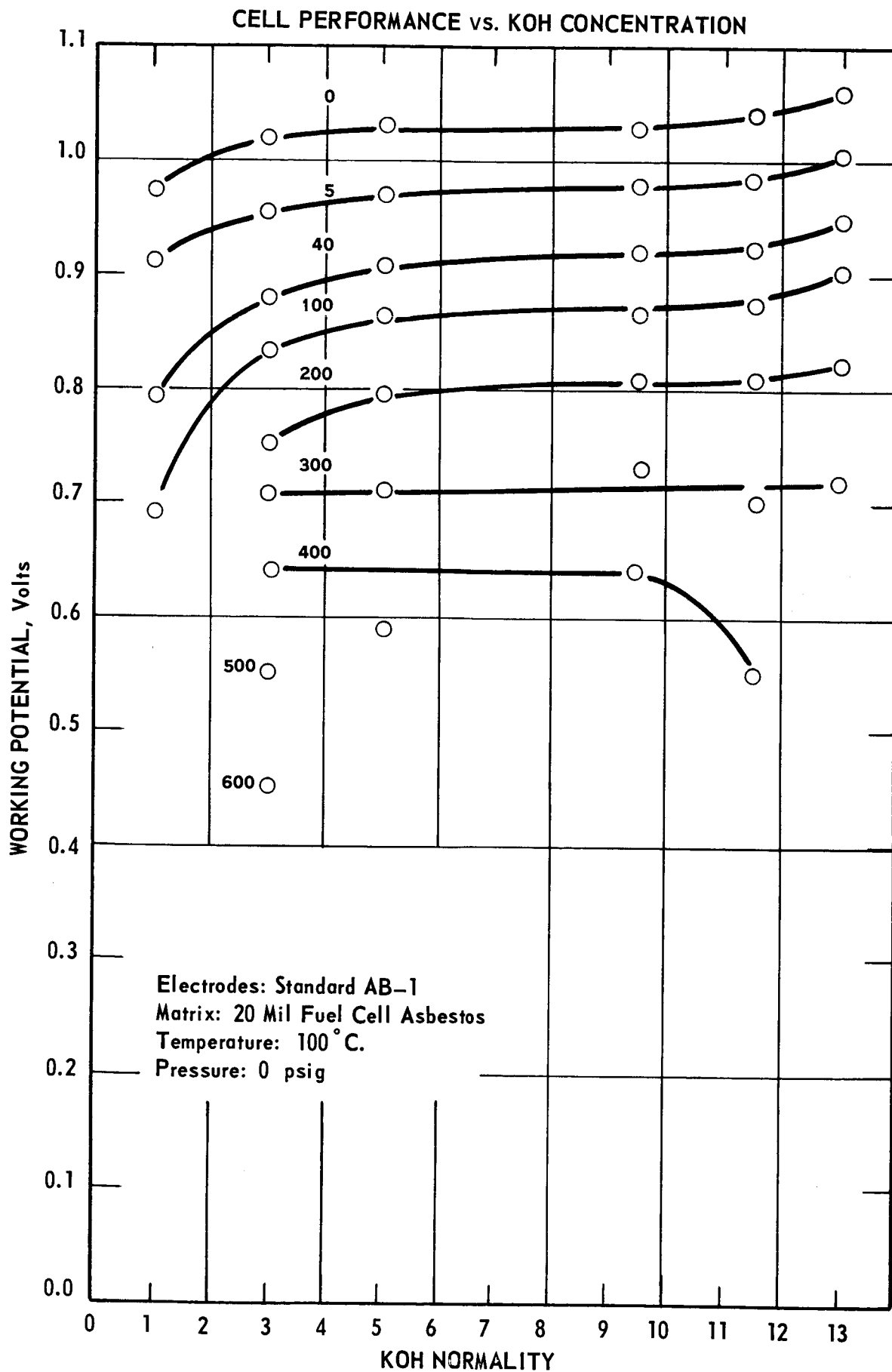


FIGURE 5-8

CELL PERFORMANCE vs. KOH CONCENTRATION

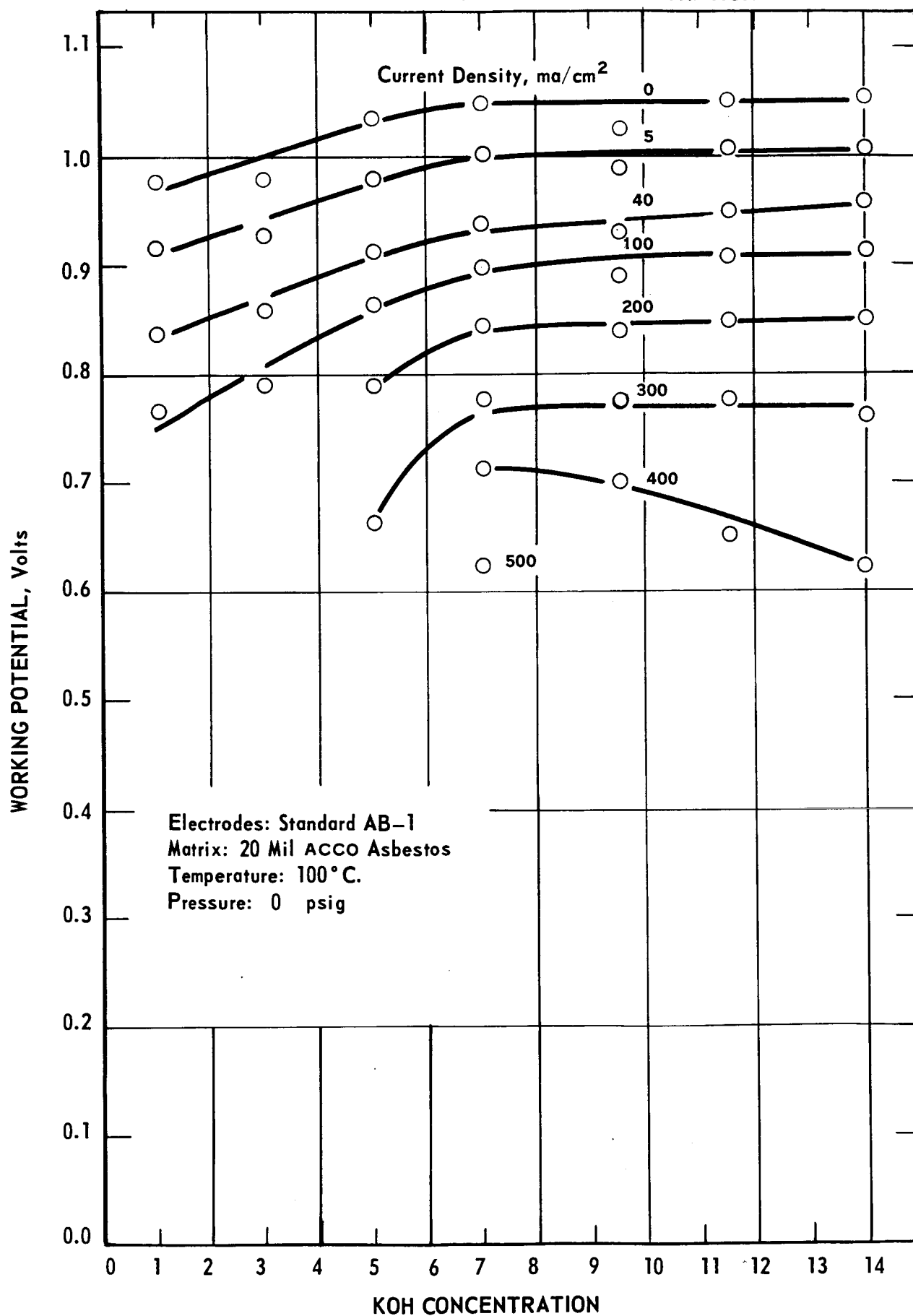


FIGURE 5-9

CELL PERFORMANCE vs. KOH CONCENTRATION

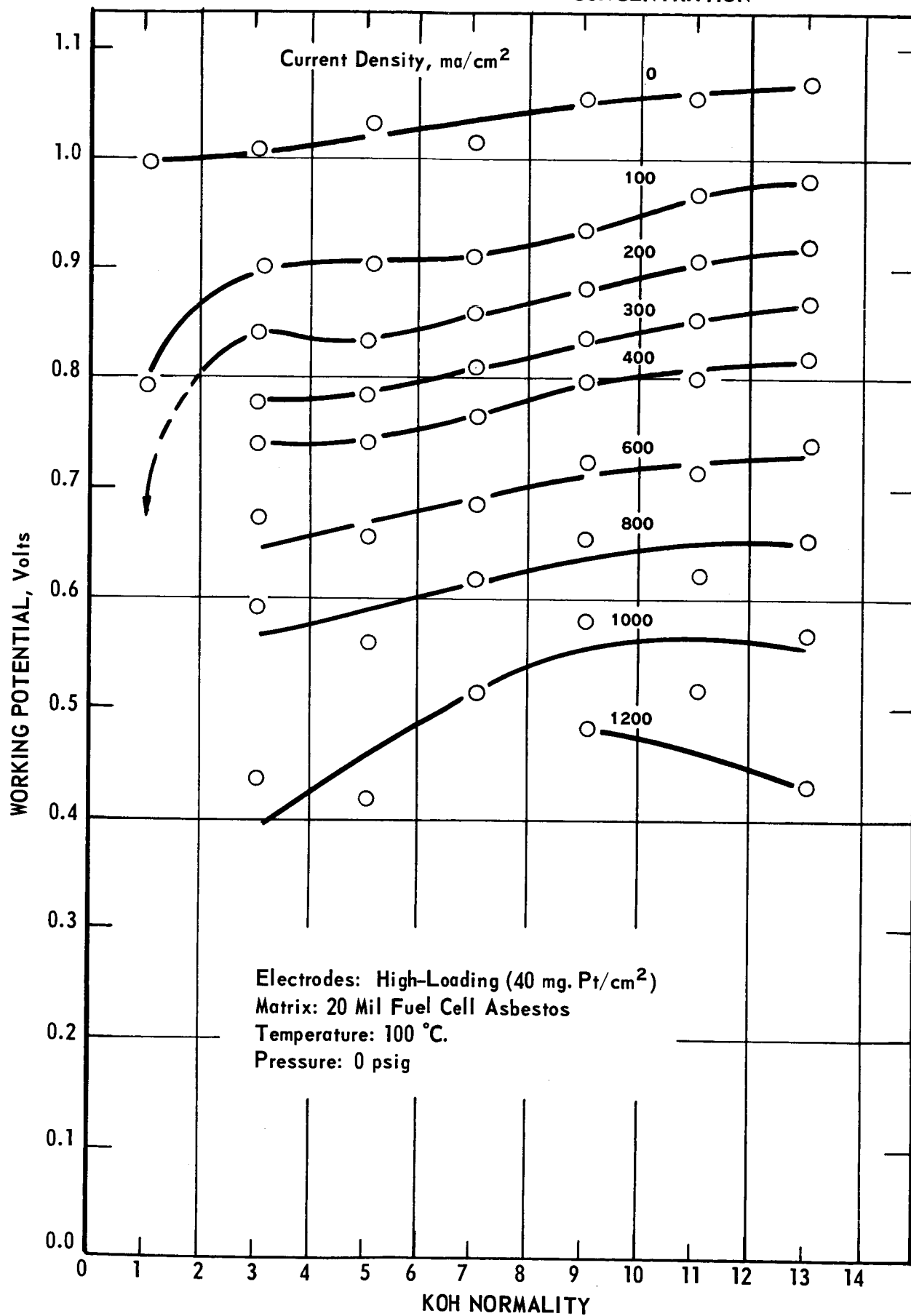


FIGURE 5-10

CELL PERFORMANCE vs. KOH CONCENTRATION

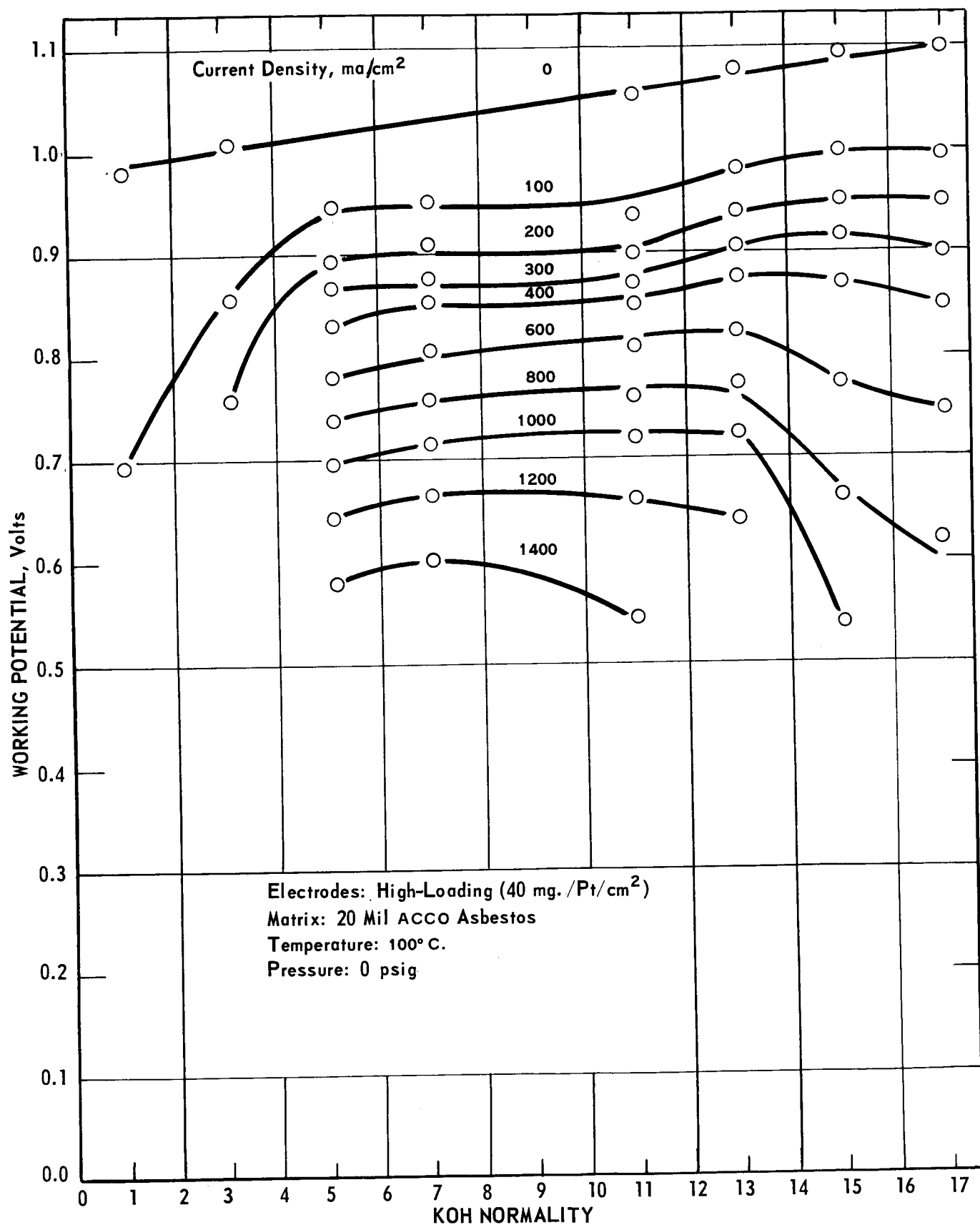


FIGURE 5-11

The following conclusions may be drawn:

(1) In the concentration range 5-13N, cell performance in all four systems increased with increasing concentration at all current densities except for current densities at or very close to the maximum. Depending upon the system and current density, the voltage increases ranged from 20-90 millivolts. These voltage increases were not caused by decreases in cell resistance since at 5-13N, cell resistance was either constant or even increased slightly (Figure 5-7). Furthermore, only a part of the voltage increase reflects the theoretical rise in reversible emf (20 millivolts) over this concentration range. It appears then that increased KOH concentration may lead to improved performance by decreasing activation or gas diffusion polarization.

(2) Cell performance decreased sharply at concentrations below 3-5N depending upon the matrix. In this concentration range, current densities of only 100-200 ma/cm² were attained. At 1N, this decrease was due partly to low electrolyte conductivity resulting in higher cell internal resistance (Figure 5-7). This is not the case at 3N KOH. The low maximum current density at 3N with ACCO Asbestos may be due to diffusion limitations caused by low partial pressures of reactant gases (100 mm Hg). At 70°C, the reactant gas partial pressure is 560 mm Hg and current densities up to 1400 ma/cm² could be attained. (This view is further supported by the effect of total pressure, described in Section 5.1.4.)

(3) At 13-17N (Figure 5-11) voltages were little affected by concentration at current densities up to 400 ma/cm². At higher current densities, voltages decreased with increasing concentration probably because at these concentrations (17N = 61% KOH, which approaches the solubility limit of KOH at 100°C, 65%), the conductivity of KOH solutions decreases sharply.

Raising the temperature, thereby increasing the electrolyte conductivity, allowed maintenance or improvement of cell performance at higher KOH concentrations. Performance at very high concentrations and temperatures is discussed in more detail in section 5.1.6.

5.1.4 Pressure

With ACCO Asbestos as the matrix, the maximum current density at 1 atm., 100°C, and 3N KOH was 200 ma/cm². Increasing the total pressure at each electrode to 1.5 and 2 atm. increased the maximum current density to 600 and 1200 ma/cm², respectively, and substantially increased the voltage at stable current densities (Table 5-2). This suggests that at 1 atm., the rate of diffusion of the reactants is limiting; the relatively low reactant partial pressure (100 mm Hg) caused by the high water vapor pressure, may lead to high gas concentration polarization. This view is supported by the magnitude of the voltage increase with increased pressure at stable current densities, 60-130 mv, which is considerably higher than the theoretical 20 mv increase in the reversible emf for an increase in pressure from 1 to 2 atmospheres.

5.1.5 Temperature

The effect of temperature in the range 50-100°C on cell internal resistance is shown in Figure 5-12 for High-Loading electrodes and ACCO Asbestos at 5N and 13N KOH. It may be noted that at the higher concentration, resistance decreased more rapidly with temperature increase. At both 5N and 13N, the resistance-temperature curves parallel the equivalent curves for free electrolyte, indicating that the observed decrease in cell resistance with increasing temperature was caused solely by the increase in conductivity of the electrolyte.

TABLE 5-2

Effect of Pressure on Cell Performance

High-Loading Electrodes - ACCO Asbestos Matrix (20 Mil) - 100°C - 3N KOH

One-Inch Cell

Absolute Pressure (ATM)	Working Voltage At Current Density (ma/cm ²) of							
	<u>100</u>	<u>200</u>	<u>300</u>	<u>400</u>	<u>500</u>	<u>600</u>	<u>800</u>	<u>1200</u>
1.0	.86	.76	*	*	*	*	*	*
1.5	.87	.83	.78	.74	.67	.58	*	*
2.0	.92	.89	.86	.83	.81	.78	.73	.61

*Current Did Not Hold

CELL INTERNAL RESISTANCE vs. TEMPERATURE

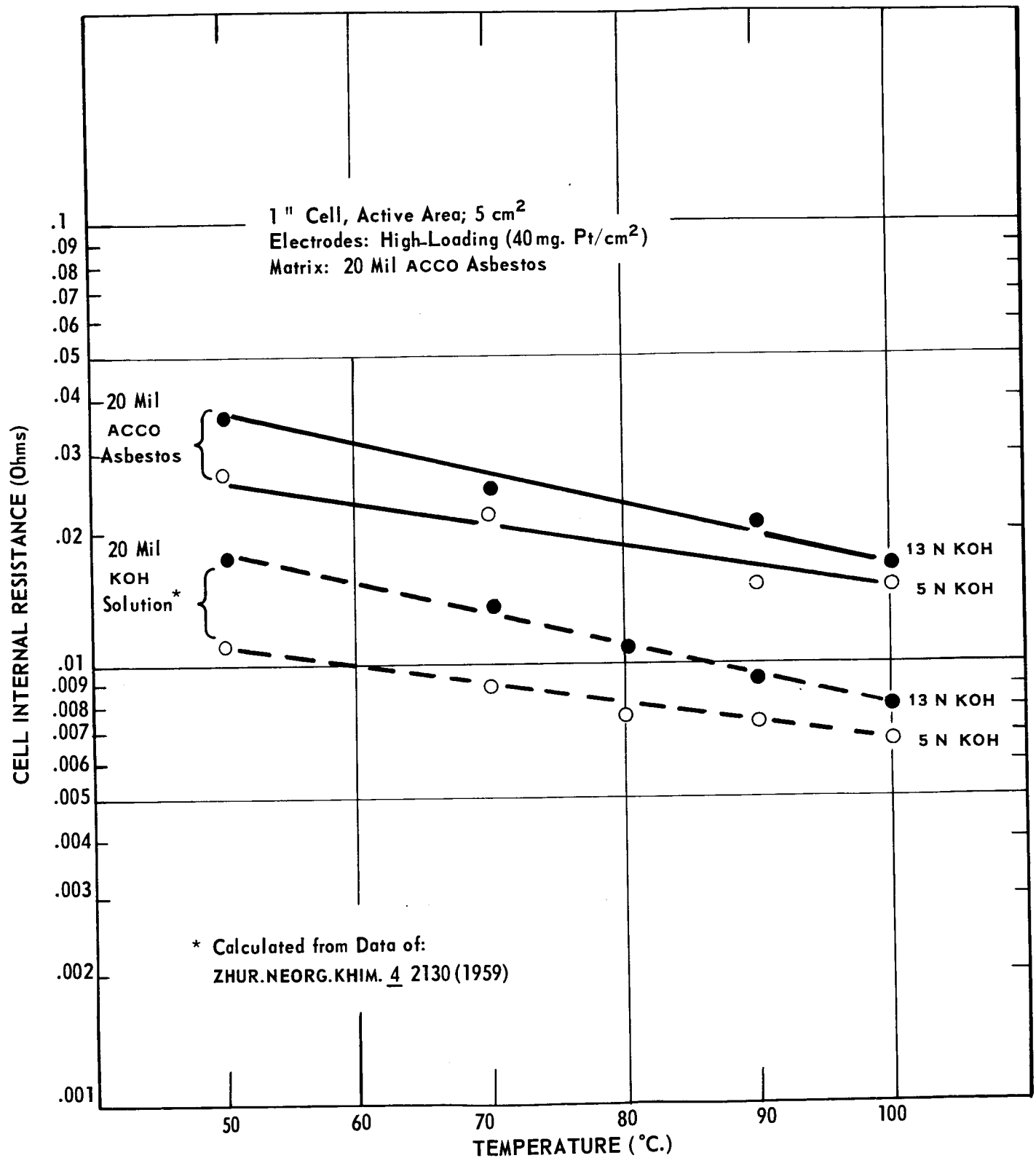


FIGURE 5-12

Figures 5-13 and 5-14 show the dependence of cell performance on temperature for this electrode-matrix system at 5N and 13N KOH. The curves for the two electrolyte concentrations are quite similar, the higher concentration indicating, in general, somewhat better performance. At high current densities, the dependence of performance on temperature is large at temperatures up to 70-80°C. Above this temperature, performance tends to level out or increase slowly. The increase in performance with increasing temperature from 50-80°C may result from a decrease in electrolyte concentration polarization. It cannot be attributed to either reversible emf or internal resistance effects. Reversible emf is an inverse function of temperature, as reflected by the slight decrease in open circuit voltage with increasing temperature (Figures 5-13 and 5-14). Decreased internal resistance accounted for only 5-25% of the voltage increase at both KOH concentrations and all current densities. At 50°C, electrolyte concentration polarization was severe enough to limit the maximum current density to 600 ma/cm², compared to 1000-1400 ma/cm² at 70-100°C.

As with the High-Loading electrode - ACCO Asbestos matrix system, the performance of the other three systems generally increased and the cell internal resistance generally decreased with increasing temperature (70-100°C). This is shown in Table 5-3 at 5N and 13N KOH. Again the temperature effect was more pronounced at the higher electrolyte concentration.

Performance of High-Loading electrodes at temperatures above 100°C is discussed in Section 5.1.6.

CELL PERFORMANCE vs. TEMPERATURE: 5N KOH

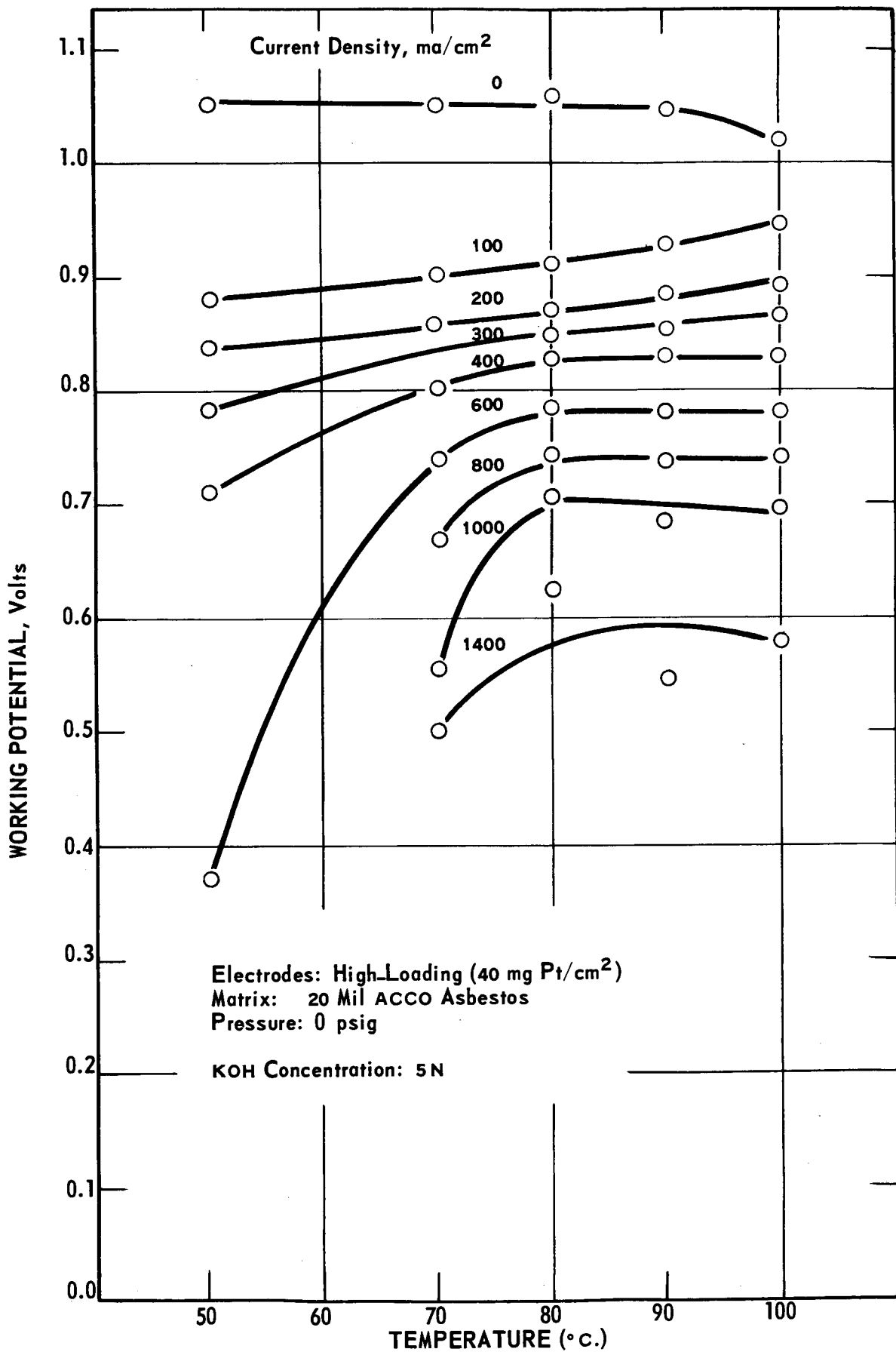


FIGURE 5-13

CELL PERFORMANCE VS. TEMPERATURE: 13N KOH

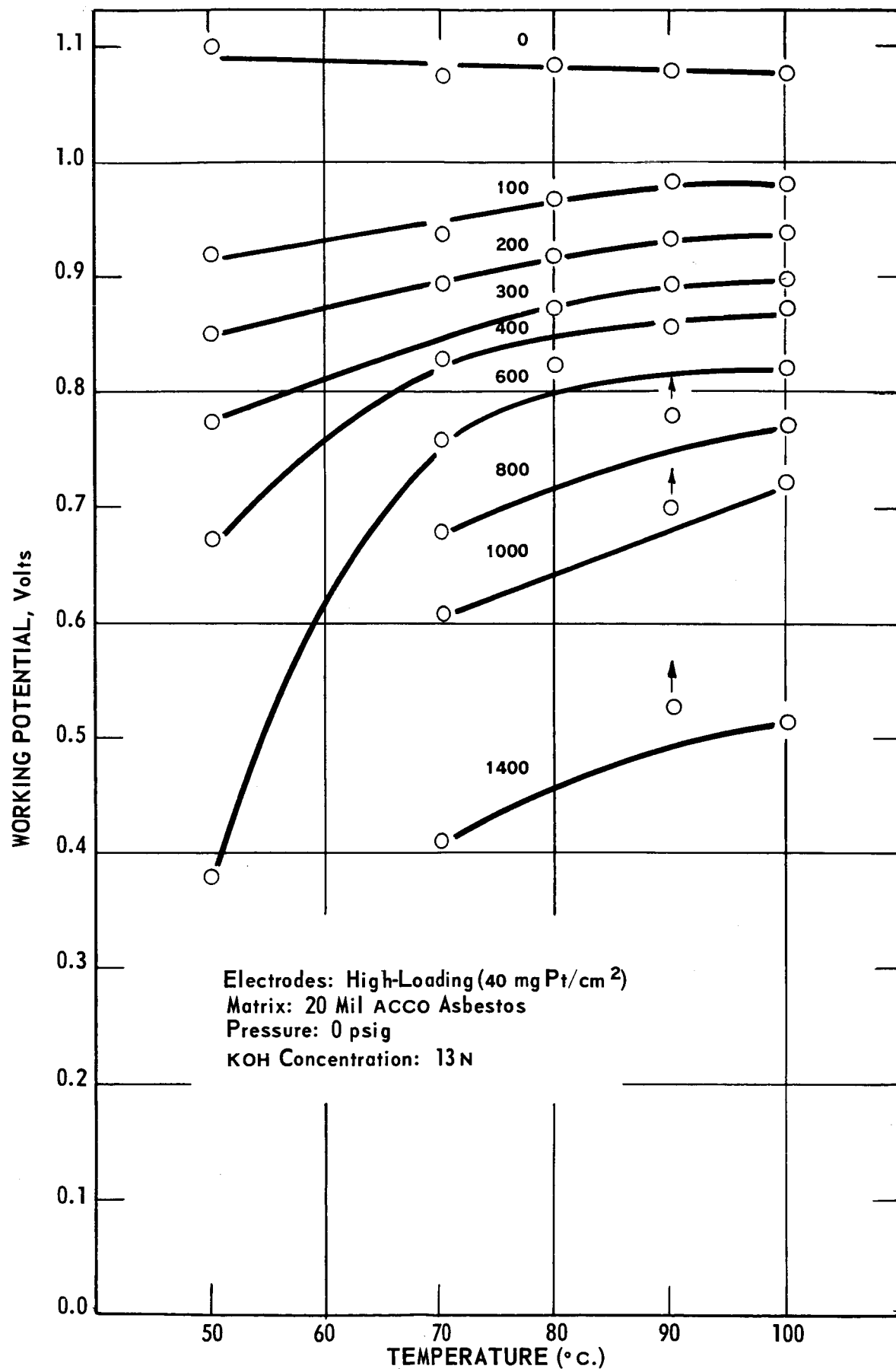


FIGURE 5-14

TABLE 5-3
Cell Performance Vs. Temperature

System Electrode, Matrix	KOH conc. (N)	Temp. (°C.)	One-Inch Cell		Working Voltage at Current Density (ma/cm ²) of:						
			Cell Resistance (OHMS)	0	100	200	400	600	800	1000	1400
Standard AB-1, Fuel Cell Asbestos	5	70	.040	1.02	.86	.80	.68	*	*	*	*
	5	100	.035	1.03	.86	.80	.59	*	*	*	*
	13	70	.055	1.08	.88	.75	*	*	*	*	*
	13	100	.043	1.06	.90	.82	*	*	*	*	*
Standard AB-1, ACCO Asbestos	5	70	.023	1.02	.88	.82	.73	.58	*	*	*
	5	100	.015	1.04	.86	.79	*	*	*	*	*
	13	70	.030	1.08	.88	.75	*	*	*	*	*
	13	100	.025	1.06	.92	.85	.63	*	*	*	*
High - Loading, Fuel Cell Asbestos	5	70	.050	1.06	.88	.82	.72	.62	.48	.36	*
	5	100	.032	1.03	.90	.84	.74	.66	.56	.42	*
	13	70	.060	1.05	.87	.82	.70	.58	.45	*	*
	13	100	.037	1.07	.98	.92	.82	.74	.65	.57	*
High-Loading, ACCO Asbestos	5	70	.023	1.04	.90	.86	.80	.74	.67	.56	.50
	5	100	.015	1.02	.94	.89	.83	.78	.74	.70	.58
	13	70	.023	1.08	.94	.90	.83	.76	.68	.61	.41
	13	100	.016	1.08	.98	.94	.88	.82	.77	.72	*

* Current did not hold

5.1.6 High Temperature and Electrolyte Concentrations

As discussed in Sections 5.1.3 and 5.1.5, performance generally improves with increasing temperature and electrolyte concentration. However, at a given temperature, performance appears to be limited by increasing ohmic polarization as concentration is increased, while at a given concentration, gas diffusion limitations become evident as the temperature is increased. Therefore, some exploratory studies were made in which both temperature and concentration were raised to very high levels.

High-Loading electrodes and ACCO Asbestos were used in these tests. The data are summarized in Table 5-4. At 120°C, voltages were essentially independent of concentration at current densities up to 300 ma/cm². At higher current densities, performance with 18N KOH was poorer than at 13N. At 140°C, performance generally increased with increasing KOH concentration from 15-19N over the entire range of current densities. In the range 100-400 ma/cm², performance at 140°C with 19N KOH was the highest so far observed for atmospheric operation. This high performance probably results in part from the rapid increase in the reversible emf as KOH concentration is increased above 15N.⁽⁴⁾

5.1.7 Electrode and Matrix Type

The performance data discussed above show that High-Loading electrodes (40 mg Pt/cm²) give higher initial performance at all current densities than do standard AB-1 electrodes (9 mg Pt/cm²), with either ACCO Asbestos or Fuel Cell Asbestos, and at all combinations of matrix thickness, cell assembly pressure, electrolyte loading, electrolyte concentration and temperatures which were studied. The range of current densities over which the variation of voltage with KOH concentration is relatively small is considerably greater for High-Loading electrodes (up to 1200 ma/cm²) than for Standard AB-1 electrodes (up to 300 ma/cm²). Thus, High-Loading electrodes

TABLE 5-4

Cell Performance at High Temperatures and Concentrations

One-Inch Cell, 1 Atm. Pressure
High-Loading Electrodes, ACCO Asbestos Matrix (20 Mll)

Temperature (°C)	Normality KOH	Working Voltage At Current Density (ma/cm ²) of									
		0	100	200	300	400	500	600	800	1000	1200
120	13	1.05	.98	.94	.90	.87	.85	.82	.77	.66	-
	18	-	.98	.94	.90	.85	.80	.75	.63	.50	.40
140	15	-	1.00	.95	.90	.86	.83	.79	.72	.64	.51
	16	-	.98	.94	.90	.88	.85	.82	.74	.67	.56
	17	1.05	.98	.96	.93	.90	.88	.84	.77	.73	.59
	19	1.12	1.02	.99	.95	.92	.88	.84	.76	.61	.53

should be able to operate at higher current densities with less difficulty from voltage changes caused by KOH concentration fluctuations during sustained operation.

The ACCO Asbestos matrix generally gives higher initial performance than does an equal thickness of Fuel Cell Asbestos, with either Standard AB-1 or High-Loading electrodes, at nearly all combinations of the operating variables mentioned above.

On the basis of initial performance, the High-Loading electrodes - ACCO Asbestos matrix system appears to be the best of the four. Life-testing is in progress to determine the comparative long-term stability of these systems.

5.1.8 Carbonate Concentration

Some additional data have been obtained on the effect of carbonate concentration on initial cell performance. These data, together with data previously reported, are summarized in Table 5-5. It appears that in the range 0-200 ma/cm², performance is governed largely by the total KOH concentration, and for KOH concentrations above 15%, is little affected by the presence of additional K₂CO₃ up to 15%. The data indicate that for an operating cell in which the initial electrolyte concentration was 30% KOH (7N), approximately half of the KOH could be converted to carbonate without a loss in performance of more than 40 or 50 mv at 100 to 200 ma/cm². On the other hand, conversion of more than half of the KOH to carbonate might well cause a major loss in performance simply because the KOH concentration would then be too low.

Analyses for carbonate were made on the matrices from two life tests run during this period. Both tests, 2-29 and 2-32, were run at 400 ma/cm², and used high gas flow rates. These analyses indicated that approximately 5-10% of the KOH originally present had been converted to carbonate.

TABLE 5-5

Effect of Carbonate Concentration on Cell Performance

Electrodes: Standard AB-1 (9 Mg Pt/Cm²)
Matrix: 20 Mil Fuel Cell Asbestos
Temperature: 70°C
Pressure: 1 Atm.

Wt.% <u>KOH</u>	Wt.% <u>K₂CO₃</u>	<u>Volts at Indicated Current Density</u>			
		<u>40</u>	<u>50</u>	<u>100</u>	<u>200</u> <u>ma/cm²</u>
15	0	.875	-	.825	.76
16.5	7	-	.885	.835	.76
19	15	-	.90	.84	.77
23	0	-	.89	.845	.775
27	6	-	.91	.86	.765
30	3	-	.915	.875	.81
30	0	.91	-	.865	.80
34	0	-	.915	.875	.81
38.5	0	.925	-	.875	.79

This level of carbonate would not account for the rapid decline in performance observed in these tests. Carbonate analyses on tests which have run for longer periods of time are in progress.

5.2 Life-Testing

Life tests conducted during the third quarterly report period are summarized in Table 5-6. During this period, increased emphasis was placed on the evaluation of High-Loading electrodes, and on testing at higher temperatures (100°C) and higher current densities (up to 400 ma/cm²). Tests in which inert materials such as platinum and Teflon were substituted for nickel cell parts were run to determine whether corrosion of the latter might be a factor contributing to the slow decline in performance generally observed in the life-testing program.

5.2.1 Used Electrodes

(1)
It has been previously reported that Standard AB-1 electrodes, when washed and reassembled in a new cell following life-testing at 70°C, give polarization data equivalent to that for fresh electrodes. To determine whether there may have been any change in the stability of operation, a pair of electrodes that had been life tested for 1000 hours (2-27) was washed and installed in a new cell for further testing (2-36). The electrode that was previously used as the H₂ electrode was retained as the hydrogen electrode. As shown in Table (5-7), the two tests appear quite similar except for the voltage decline after 750 hours total elapsed time. It is suspected that the high decline rate at the end of the second test may have been due to a poor water balance.

5.2.2 High-Loading Electrodes

Several tests were run with High-Loading (40 mg Pt/cm²) electrodes, using dry feed gases at 70°C. Test 2-43, which was terminated after 1032 hours, showed the high initial performance typical of

TABLE 5-6

Life Test Summary (2" x 2" Cells)

Test Notebook No.	Cell Design (1)	(2)		Current Density (ma/cm ²)	Matrix	Initial H ₂ Conc. (g)	Inlet Gas Condition	Inlet Gas Flow Ratio, H ₂ /O ₂	Test Duration (hrs.)	Status	Cell Voltage		Remarks
		Electrodes	Pt Loading (mg/cm ²)								Initial	Max.	
2-17, 6708-19	I	9 (AB-1)		100	FOAB ⁽⁴⁾ -30	7.2	Dry	0.7	2245	Terminated	.843	.847	Gases reversed @ 808, 1850 hrs.
2-24, 6708-57	II	"	"	"	FOAB-20	"	"	0.7	3374	Continuing	.845	.845	Gases reversed @ 50, 613, 2100, 3205 hrs.
2-31, 6597-42	"	"	"	"	FOAB-30	5.0	{ H ₂ : Sat. @ 47°C O ₂ : Dry	13.0 ⁽⁵⁾	1223	Terminated	.822	.822	.77
2-27, 6597-26	"	"	"	"	"	7.2	Sat. @ 47°C	0.6	1014	"	.800	.844	.79
2-36, 6597-58	"	"	(used) ⁽⁶⁾	"	"	5.0	"	0.8	1012	"	.665	.834	.74
2-47, 6597-94	"	"	"	"	FOAB-20	8.0	Dry	1.1	143	"	.876	.876	.806
2-48, 6597-95	"	"	"	"	"	"	"	1.1	161	"	.883	.889	.886
2-50, 6597-100	"	"	"	"	"	"	"	1.1	380	"	.876	.882	.842
2-30, 6708-76	"	"	"	"	ACCO B-2 ⁽⁷⁾	5.0	"	0.8	1317	"	.891	.891	.815
2-29, 6597-33	I	"	"	400	FOAB-20	"	"	0.8	338	"	.715	.715	.534
2-32, 6597-44	"	"	"	"	"	"	Sat. @ 50°C	0.8	112	"	.666	.666	.558
2-33, 6708-111	II	"	"	100	"	7.1	Sat. @ 70°C	1.2	1030	"	.849	.849	.817
2-51, 6597-106	"	"	"	"	ACCO Asbestos ⁽⁸⁾	8.0	"	1.4	212	"	.880	.904	.75
2-43, 6597-80	II	40	"	100	FOAB-20	8.0	Dry	1.1	1032	Terminated	.880	.888	.790
2-54, 6597-120	"	" (Exp. Ni support screen)	"	"	"	"	"	1.1	234	Continuing	.906	.907	.862
2-38, 6597-66	"	" (14% Teflon)	"	"	"	5.0	"	1.2	779	Terminated	.848	.854	.818
2-57, 6597-114	"	"	"	"	ACCO Asbestos	8.0	"	1.1	186	Continuing	.895	.902	.889
2-34, 6597-54	I	"	"	400	" (un-leached)	5.0	Dry	0.8	295	Terminated	.794	.794	.641
2-40, 6597-74	"	"	"	"	"	"	"	1.1	1105	Continuing	.778	.778	.60
2-59, 6597-108	II	"	"	100	FOAB-20	8.0	Sat. @ 70°C	1.0	138	"	.840	.868	.690
2-45, 6597-92	"	"	"	"	ACCO Asbestos	"	"	1.5	354	Terminated	.871	.901	.73
2-42, 6708-147	II	10 (50% Teflon)	"	100	FOAB-20	8.0	Dry	1.1	835	Terminated	.822	.847	.73
2-39, 6708-129	II ⁽⁹⁾	" (Pt Support Screen)	"	"	"	7.2	"	1.3	1110	"	.867	.869	.72
2-46, 6597-83	II	"	"	"	"	8.0	"	1.1	738	Continuing	.876	.876	.861
2-56, 6708-152	II ⁽⁹⁾	"	"	200	"	"	"	1.1	143	Terminated	.824	.824	.72
2-60, 6708-155	II ⁽⁹⁾	"	"	"	"	"	"	1.2	64	Continuing	.788	.809	.796
2-53, 6708-134	II	" (Teflon support screen)	"	100	"	"	"	1.0	234	"	.831	.840	.831

(5) Slow oxygen purge; essentially all water removal on hydrogen side.
 (6) Same electrodes as in Test 2-27.

(7) Proprietary Cyanamid membrane.

(8) Proprietary Cyanamid Asbestos matrix.

(9) Platinum spacer screens, and platinum foil lining nickel face plate.

(1) Cell design I uses Teflon-covered silicone rubber gaskets and flat spacer screens. Cell Design II uses solid Teflon gaskets and corrugated screens

(2) Teflon level was 25% except as otherwise indicated.

(3) Voltage as of July 31, 1964, or at termination of test.

(4) Johns Manville Fuel Cell Asbestos in nominal .30 or .20 mil thickness.

TABLE 5-7

Life Test of Used Electrodes

	<u>Test 2-27</u> <u>(New Electrodes)</u>	<u>Test 2-36</u> <u>(Used Electrodes)</u>
Starting	0.800 v ⁽¹⁾	0.660 v ⁽¹⁾
Maximum Voltage	0.844 v	0.833 v
Average Voltage Decline:		
100-750 hrs.	5 mv/100 hr.	5 mv/100 hr.
750-1000 hrs.	9 mv/100 hr.	23 mv/100 hr.
Minimum Cell Resistance	10.8 milliohms	15.0 milliohms
Average Resistance		
Rise During Test:	1 milliohm/100 hr.	0.7 milliohm/100 hr.

(1) Low initial voltage due to high initial electrolyte loading

High-Loading electrodes. A downward trend in voltage (10 mv/100 hrs.) and an upward trend in cell internal resistance (1.8 milliohms/100 hrs.) similar to those previously observed in tests with Standard electrodes were also noted. In life test 2-57, High-Loading electrodes are being used with an ACCO Asbestos matrix, and in life test 2-54, High-Loading electrodes having expanded metal rather than woven-wire nickel support screens are being tested. Over the first several hundred hours of these latter tests, performance trends are similar to those in life test 2-43, although in the test with the expanded nickel support screens, voltage appears to be dropping somewhat more rapidly.

In other tests, High-Loading electrodes were evaluated at 100°C, and at high current densities (400 ma/cm²). These tests will be described in later sections of this report.

5.2.3 Matrix Variations

Throughout most of the life-testing program, Johns-Manville Fuel Cell Asbestos has been used as a standard matrix material. However, ACCO Asbestos⁽¹⁾ appears to offer a possible advantage in terms of higher performance, particularly at high current densities. This matrix has, therefore, been used in several life tests to determine its stability over long periods of time. Earlier in the program⁽¹⁾, relatively stable performance with ACCO Asbestos at 70°C was indicated in life test 2-3 (6582-18). In the current series of tests, ACCO Asbestos has been used at 70°C with High-Loading electrodes in tests run at both 100 and 400 ma/cm². Life test 2-57, at 100 ma/cm², has run well for 186 hours

Life test 2-40 has run for 1105 hours at 400 ma/cm², and is continuing, although at a relatively low performance level (ca. 0.50 v). These tests indicate that ACCO Asbestos probably has adequate stability at 70°C. Several tests with ACCO Asbestos at 100°C have been run (these tests are described in the following section), but stability at 100°C has not yet been demonstrated.

5.2.4 Tests at 100°C

Four tests have been run at 100°C, using Standard AB-1 and High-Loading electrodes, Fuel Cell Asbestos and ACCO Asbestos. In all tests, the inlet gases were saturated with water at 70°C. Life test 2-33, with AB-1 electrodes and Fuel Cell Asbestos, operated very stably for 1032 hours. As shown in Figure 5-15, voltage decline (about 3 mv/100 hrs.) and resistance rise (0.7 milliohms/100 hrs.) were quite low. Good control of water balance is indicated in this test by the general smoothness of the voltage and resistance curves.

The three other tests at 100°C in this series all exhibited a sharp decline in voltage and rapid rise in resistance and were terminated after only a few hundred hours. Two of these tests used ACCO Asbestos (2-45 and 2-51); the other (2-59) used Fuel Cell Asbestos. The poor performance in these tests may quite likely be attributed to factors other than instability of the matrix. The electrodes from life test 2-45 were washed and reevaluated. There was no loss in performance as compared to fresh electrodes. Thus, if there has been any degradation of the ACCO Asbestos at 100°C, it has not caused any permanent deactivation of the electrodes.

LIFE TEST 2-33 @ 100 °C.

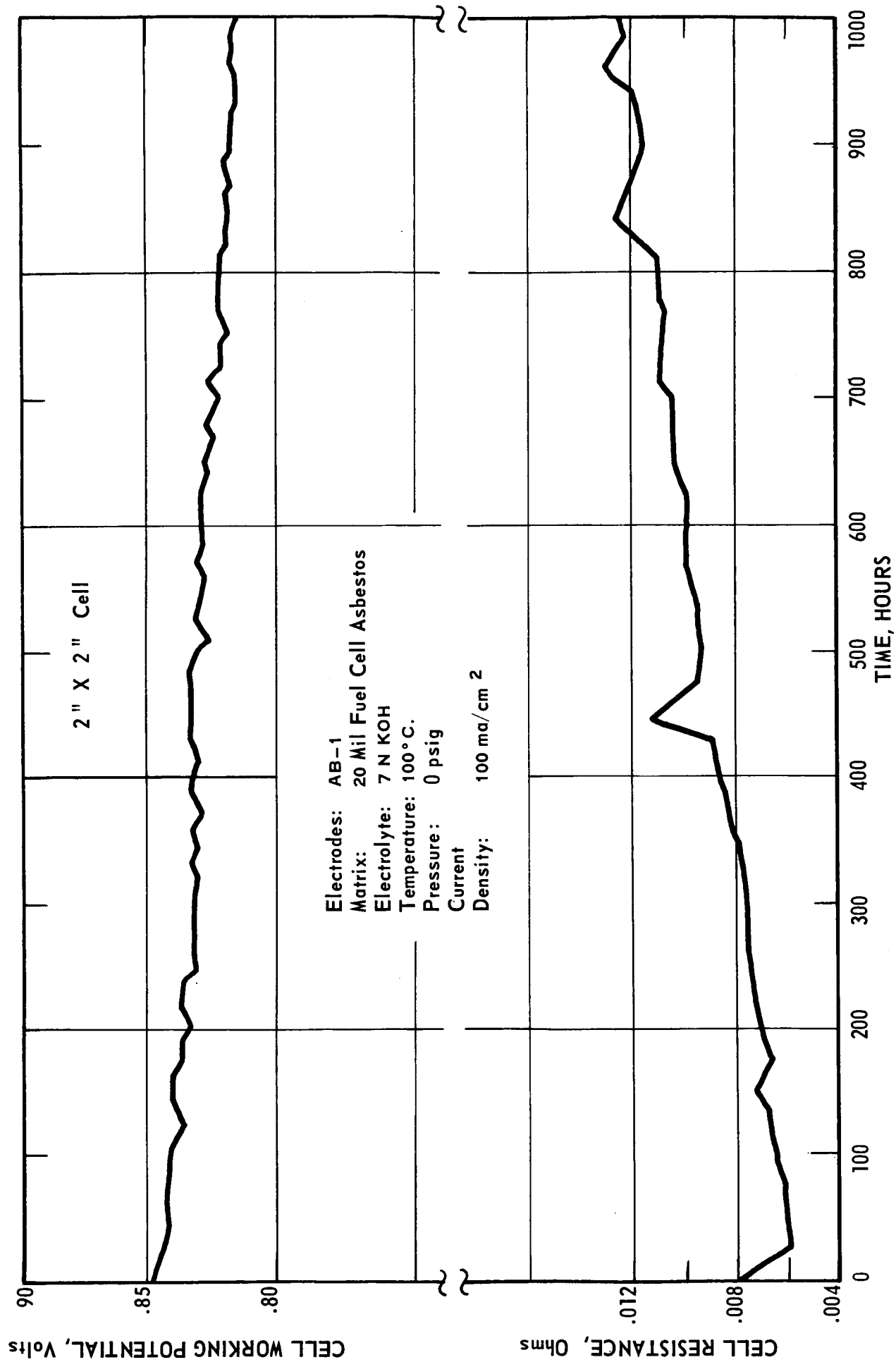


FIGURE 5-15

Testing at 100°C will continue in order that more definite conclusions with respect to electrode and matrix stability may be drawn.

5.2.5 High Current Densities

In order to determine which electrode - matrix system and combination of operating conditions would be most satisfactory for operation at relatively high current densities, a series of life tests at 400 ma/cm² was run. The tests were made at 70°C and 0 psig, using 5N KOH. Two tests were run with Standard AB-1 electrodes and Fuel Cell Asbestos, using dry gases in one case (2-29) and saturated gases in the other (2-32). Two other tests were run with High-Loading electrodes and ACCO Asbestos (2-34 and 2-40). In all these tests, there was a relatively rapid downward trend in voltage, as well as wide fluctuations within the overall trend. Interestingly, though, there was no apparent upward trend in cell resistance comparable to that observed in tests at 100 ma/cm². The tests with High-Loading electrodes and ACCO Asbestos started at a higher level and dropped somewhat less rapidly than did the tests with Standard AB-1 electrodes and Fuel Cell Asbestos. One test (2-40) was continued for over 1,000 hours. Wide fluctuations were observed indicating great difficulty in controlling the water balance at this high current density.

Two other tests (2-56 and 2-60) have been run at an intermediate current density (200 ma/cm²). These tests were run in cells having platinum electrode-support and spacer screens in place of nickel (see section 5.2.8). In one case, performance was poor and the test was terminated after 143 hours. The second test (2-60) has been running for only 64 hours, but has run stably during that period.

5.2.6 Effect of Gas Reversals

Life test 2-24 continues to run well after 337⁴ hours of operation at 100 ma/cm². In this test, the gases have been reversed (hydrogen on the oxygen side and vice-versa) four times. Slow downward trends in voltage and upward trends in cell resistance between gas reversals have been arrested by the reversals. Except for brief periods when the cell was out of water balance, voltage has been maintained between .835 and .81 volts and cell resistance between .009 and .012 ohms for 2700 hours since the first gas reversal.

5.2.7 Variations in Waterproofing Level

The standard level of waterproofing for the electrodes used in this program has been 25% Teflon. Some work reported previously⁽²⁾ indicated that electrodes with lower Teflon levels performed somewhat erratically in short term polarization tests. During the current report period, electrodes containing both lower (14%) and higher (50%) Teflon levels were life-tested. In life test 2-38, High-Loading electrodes containing 14% Teflon ran poorly for about 160 hours until the gases were reversed. Following gas reversal, the level of performance improved, but the usual trends in voltage and cell resistance were observed. In life test 2-42, electrodes having standard platinum loading (10 mg/cm²) but with 50% Teflon were tested. In this test, the initial voltage was somewhat low (0.82 v). After about 100 hours of operation, voltage began to decline and resistance to rise at an accelerated rate. These trends could not be altered by variations in gas flow rate. The gases were reversed at 330 hours, and following this reversal, both

voltage and cell resistance returned abruptly (within several hours) to normal values. The cell then ran stably for approximately 250 hours before starting another period of accelerated decline, leading to termination of the test after 835 hours. The accelerated trends in this latter test may have been due to "over-waterproofing" in the electrode. In view of these results, it does not appear desirable to change the waterproofing level from the standard 25%.

5.2.8. Platinum and Teflon Screens

In view of the beneficial effect on both voltage and resistance following gas reversals, it was felt that the observed downward trends in performance might be due at least in part to corrosion of the nickel screens used as electrode support and as spacers in the test cells. To check this hypothesis, a life test (2-39) was set up with no nickel exposed to the gases or to the electrolyte. The electrodes consisted of 10 mg Pt/cm² on platinum screen. Spacer screens were platinum and the inside surfaces of the nickel face plate were lined with platinum foil. As shown in Figure 5-16, this cell ran for 800 hours at 100 ma/cm² with no loss in voltage, and no increase in cell internal resistance. After 800 hours, performance declined rather rapidly. On disassembling the cell after shutdown, solid deposits of KOH, which interfered with electrical contact within the cell and also permitted cross-flow of gases, were observed. Thus, the decline in performance does not appear to have been directly associated with the electrodes.

The performance obtained in life test 2-39 strongly suggests that corrosion of nickel cell parts is a factor contributing to the downward performance trends generally observed in our life-testing program. To determine whether the difficulty lies in the electrode

LIFE TEST 2-39
PLATINUM ON PLATINUM SCREEN ELECTRODES

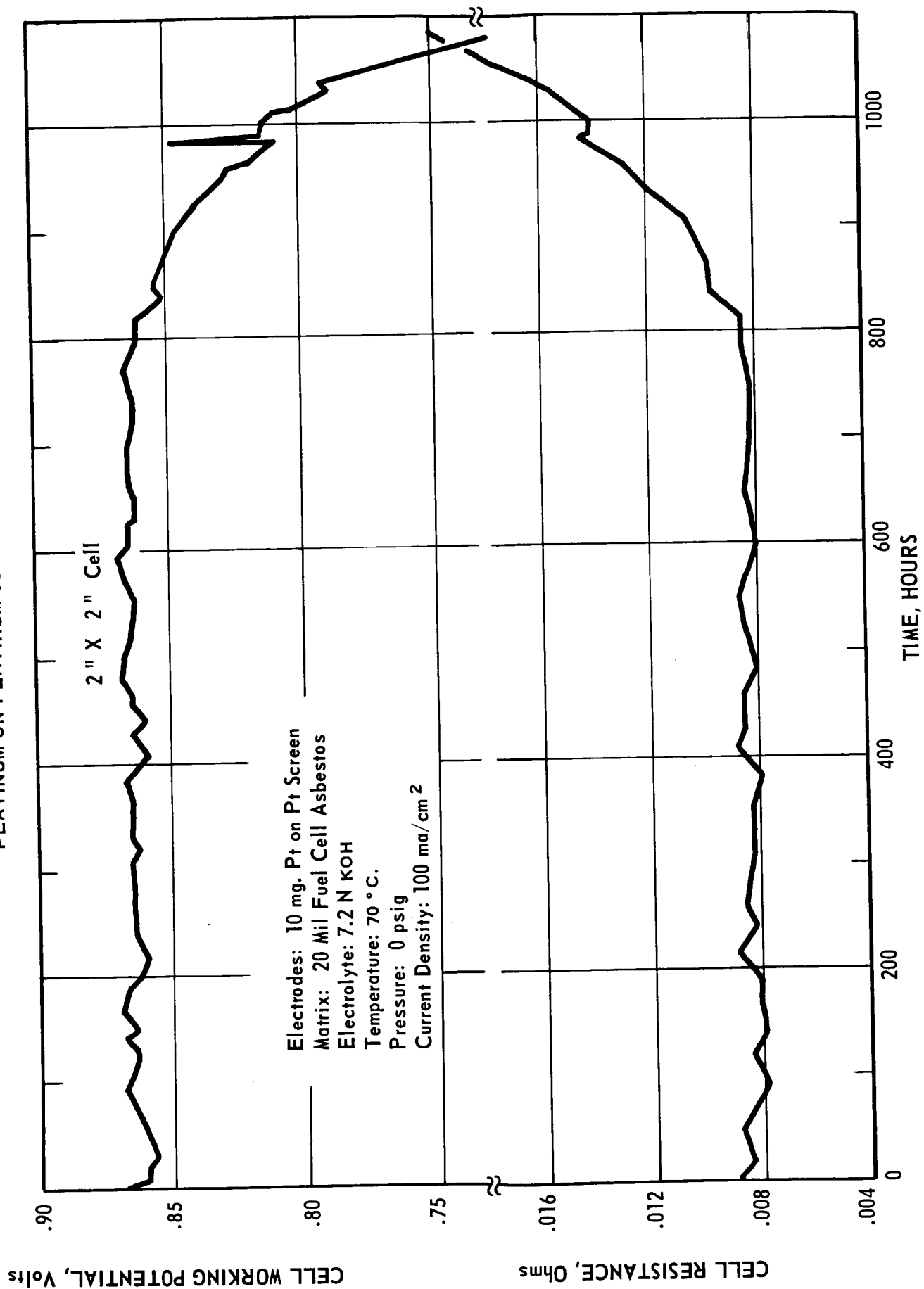


FIGURE 5-16

support screen or in other parts of the current collector circuit (spacer screens, etc.), a life test (2-46) has been set up with 10 mg Pt/cm² on platinum screen electrodes, but otherwise standard nickel parts. This cell has been running for 738 hours, and has shown only a very slight downward trend in voltage (< 2 mv/100 hrs. after the first 24 hours) and very little if any upward trend in cell resistance(< .2 milliohms/100 hrs.). It appears, therefore, that the major problem lies in the electrode support screen.

Examination of the nickel screens at the end of a life test generally shows that those at the oxygen side are tarnished, whereas those at the hydrogen side are still bright. This suggests that formation of oxide films may effect cell resistance and therefore also the voltage output. Further life tests using platinum screens only on the oxygen side of the cell are planned.

The use of woven Teflon screen to replace nickel screen as an electrode support has been considered. Although the Teflon support screen is not electrically conductive, good performance can be achieved using a close-meshed current collector screen. Figure 5-17 shows polarization data for a platinum-on-Teflon screen electrode compared with a Standard AB-1 electrode. Performance is good, although somewhat lower than the standard. A life test (2-53) utilizing platinum-on-Teflon screen electrodes has been started. For 234 hours, this test has been running stably at .83-.84 volt and .009-.010 ohms cell resistance.

POLARIZATION DATA

TEFLON-SCREEN ELECTRODES

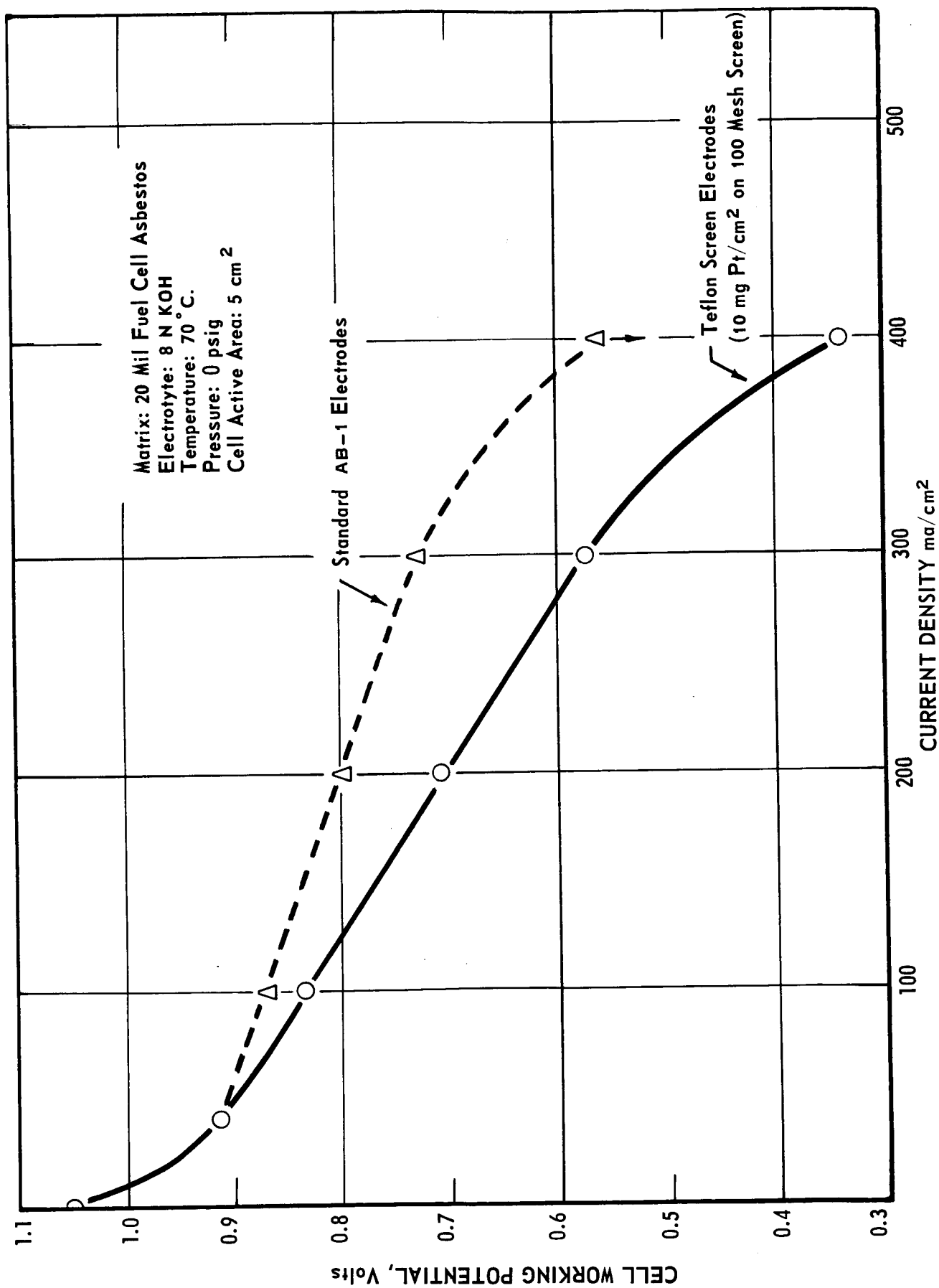


FIGURE 5-17

5.2.9 Cell Design for Life-Testing Under Pressure

A cell has been designed and constructed for operation at pressures up to 60 psig, and with differential pressures between H_2 and O_2 of at least 5 psig. Figure 5-18 shows the basic design features. The active area, as with the standard cell, is 2" x 2". Gas distribution within the active area (not shown in the figure) is also the same as in the standard cell. Sealing against cross-leakage of gas is accomplished by compression of the matrix between the lands in the grooved area surrounding the active area of the cell. The grooves permit electrolyte to be squeezed out during cell assembly, thus preventing hydraulic rupture of the matrix. Leakage of gas or electrolyte out of the cell is prevented by an O-ring seal.

Preliminary tests indicate the basic design to be satisfactory, and a life test under pressure is planned.

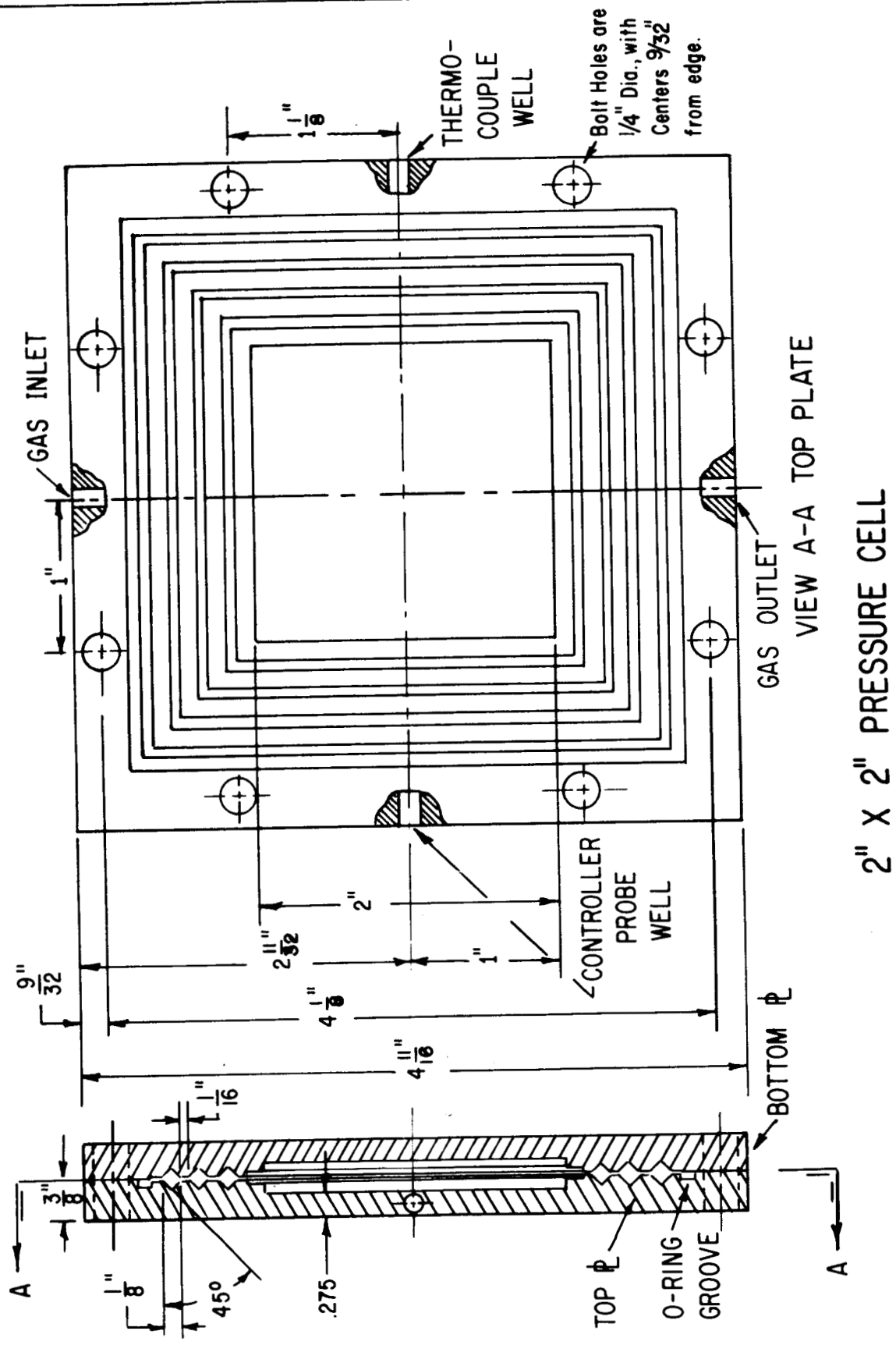


FIGURE 5-18

6. SCALE-UP

6.1 Choice of Operating Conditions

For scale-up work it is desirable to select an electrode-matrix system, cell assembly conditions, and operating conditions which will lead to minimum weight/net power of an entire battery system, including battery, all auxiliary equipment for heat and water removal and power control, and fuel plus associated tankage. Where the weight of fuel plus associated tankage is an overriding factor in system weight (long missions), maximum voltage output at reasonable current density is desired. Where fuel and associated tankage weight is not an overriding factor, calculations reported previously⁽²⁾ showed that maximum battery humidity is desirable (even though cell performance is slightly lower) because of lower weight and power consumption of equipment for removing battery heat and water.

With these two cases in mind, Table 6-1 summarizes the combination of electrode-matrix system, cell assembly, and operating conditions which the performance data described in Section 5 of this and the Second Quarterly Report indicate to be at or near the optimum. The maximum temperature considered was 100°C. The optimum gas pressure is not stated here, since work to define it is still in progress, but preliminary data show that the best operating pressure will be greater than atmospheric. Two electrolyte concentrations, 5N and 13N, are shown. The higher concentration corresponds to maximum performance and low battery humidity, hence minimum weight/net power of a battery and fuel plus associated tankage. The lower concentration corresponds to performance somewhat below the maximum but to maximum battery humidity, hence to minimum weight/net power of equipment for removing battery heat and water. The system and conditions listed in Table 6-1 will be used for scale-up work at 100-500 ma/cm².

TABLE 6-1

Operating Conditions for Scale-up

Electrodes:	High-Loading (40 mg Pt/cm ²)
Matrix:	ACCO Asbestos
Matrix Thickness:	20 mils
Cell Assembly Pressure:	150 psi
Electrolyte Loading:	2 g Solution/g Dry Matrix
Temperature:	100°C
<u>Electrolyte Concentration</u>	
Working Voltage (Atmospheric Pressure)	
at Current Density of:	
100 ma/cm ²	0.94
200	0.89
300	0.87
400	0.83
500	0.80

*Including auxiliaries, but exclusive of fuel and tankage

The data of Section 5.1.7 show that still higher initial performance may be obtained at temperatures above 100°C, particularly at KOH concentrations above the solubility limit at 100°C. Work is in progress to investigate further operation at 100-200°C and to define optimum operating conditions. It is anticipated that work in this temperature range will introduce new materials problems, particularly with respect to matrix stability.

6.2 Design of 6" x 6" Cell

A fuel cell was designed and constructed for evaluating the performance of scaled-up electrodes (6" square) at pressures above atmospheric. The nickel face plates were designed to provide uniform gas distribution over the electrodes by manifolding from a 1/4 in. diameter header through evenly spaced 1/8 in. diameter channels, and then through 1/32 in. diameter orifices spaced at 1 in. intervals along the length of each channel (Figure 6-1). Gas discharge will be through an identical manifold whose channels run parallel to and alternate with the channels of the inlet manifold. The nominal path of gas flowing through each inlet orifice over the electrodes is 1 in. Previous experimental work with 1 in. diameter and 2 in. square electrodes indicated that this path length is sufficient to saturate each gas with water vapor without causing electrolyte concentration gradients large enough to affect cell voltage adversely.

Gas distributions were measured experimentally in a plastic model of the face plates of the scaled-up cell over the entire expected range of total hydrogen and oxygen flow rates (70-8000 cc/min.). The flow rate of both hydrogen and oxygen among the manifold channels was found to vary by a maximum of 15% at 1000-8000 cc/min. total flow, and by a maximum of 20% at 70-400 cc/min. The flow rates of both hydrogen and oxygen among the rows of orifices varied by a maximum of 15% at average flows of 487-1130 cc/min. in the channels. At very low flows in the channels (15-167 cc/min.), the variation among the rows of orifices was as high as 25-30%. These experimental data indicate that gas distribution in the 6" x 6" cell will be sufficiently uniform.

6" X 6" CELL DESIGN

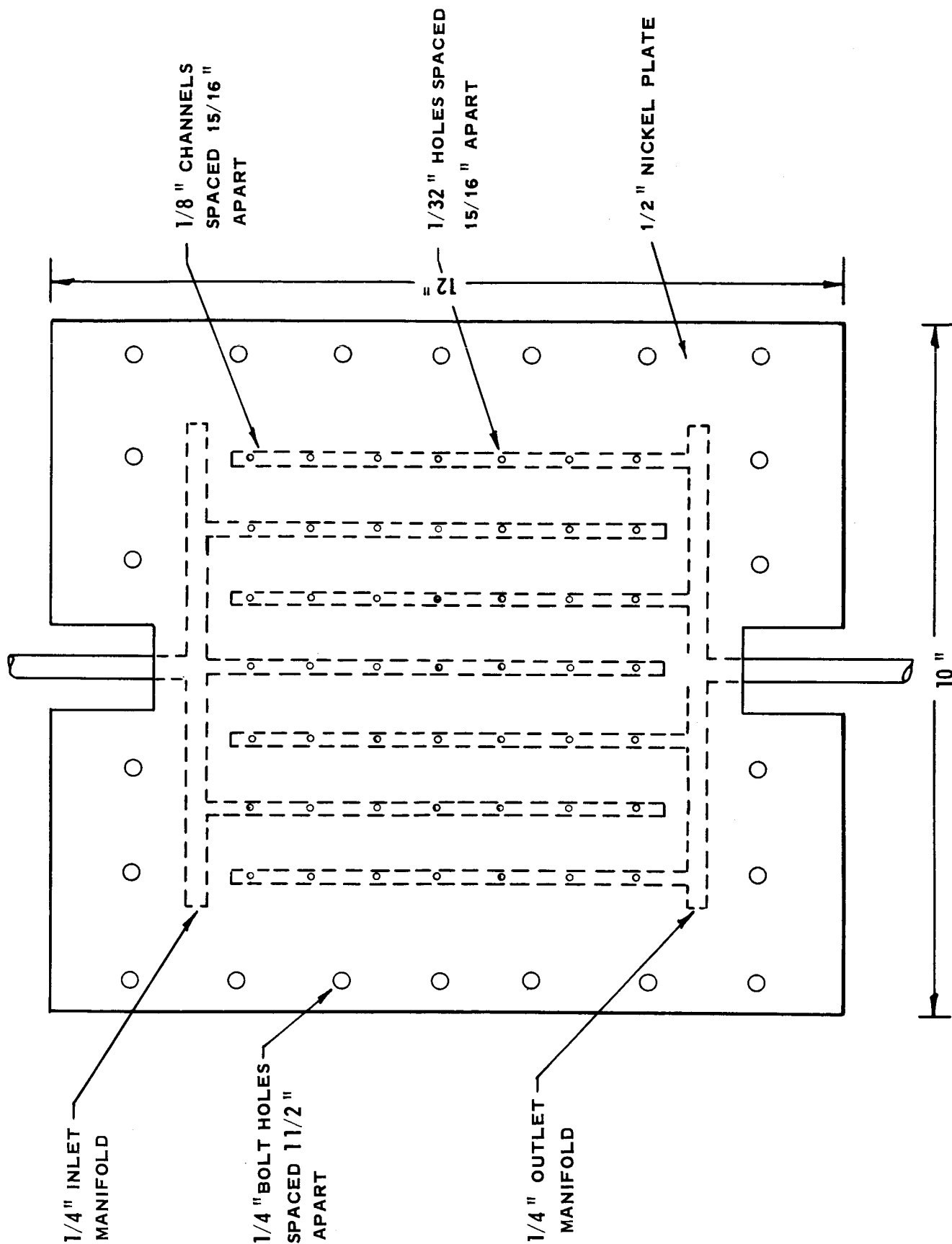


FIGURE 6-1

6.3 Mathematical Simulation of Fuel Cell Operation

As described in Section 5, the performance of a given cell assembly operated at a given total pressure depends on the electrolyte concentration, electrolyte loading, and the temperature. It is expected that during steady state battery operation, gradients in these three variables will exist over the face of the electrodes and through the thickness of the electrode-membrane sandwich. Consequently, for optimum performance of the fuel cell system, the battery should be designed and operated to limit these gradients within the boundaries defined by the data of Section 5.

The effect of battery design and system operation on the magnitude of these gradients at steady state in a battery cell was simulated by a mathematical model. General differential mass and energy balances were set up and solved for a system of dynamic water and heat removal from the battery with no auxiliary cooling. Similar calculations are in progress for a dynamic system with auxiliary cooling. The simulation is described below.

6.3.1. Development of the Model

6.3.1.1. Physical Picture and Assumptions

The actual cell design has not been chosen at this point so it will be necessary to utilize a suitable general model which can be easily adapted to different designs. The cell configuration, flow scheme, and coordinate system chosen for this simulation are shown in Figure 6-2. It is assumed that the hydrogen enters from a channel which distributes gas uniformly along the line $x = 0$. Similarly, gas is removed uniformly along the edges of the cell at $x = \frac{1}{2} a$. Equations will be written for one unit of this cell, i.e., from $x = 0$ to $x = a$. Other cell configurations, which may contain more inlet and exit channels, can then be built up from this single unit.

An actual fuel cell battery will consist of a number of individual cells in series. At present, a thirty cell, twenty-eight volt unit is envisioned. This simulation will cover a single cell in the midst of such a battery: that is, there will be no transfer of heat to adjoining cells. Referring to Figure 6-2, a single cell is composed of:

- a. the hydrogen half of the distributor plate;
- b. the hydrogen gas space, containing a screen to distribute the flow and also keep the electrode pressed against the electrolyte membrane;
- c. the hydrogen electrode;
- d. an asbestos membrane containing the electrolyte, a potassium hydroxide solution;
- e. the oxygen electrode;
- f. oxygen gas space screen;
- g. the oxygen side of the distributor plate.

CELL CONFIGURATION FOR MATHEMATICAL MODEL

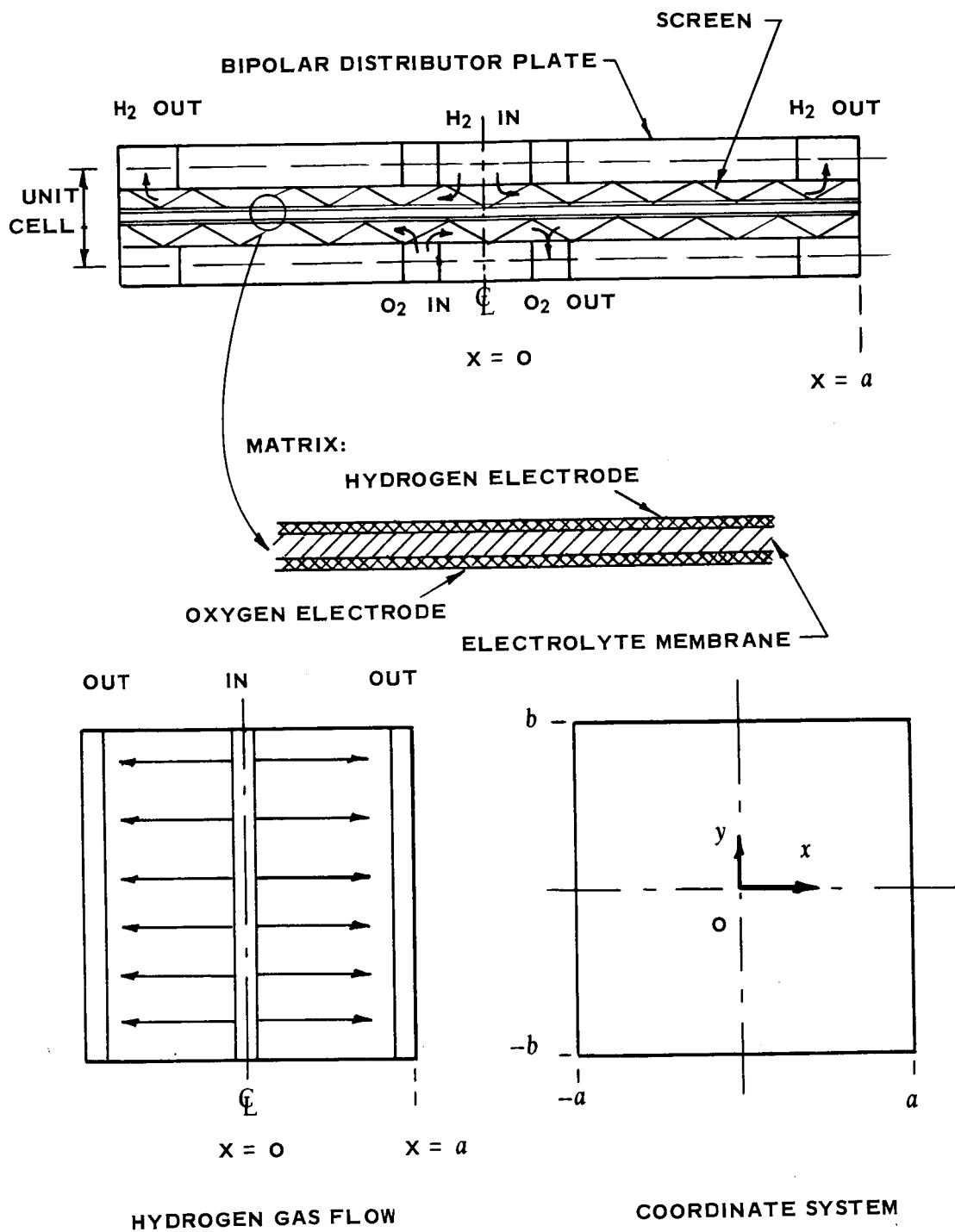


FIGURE 6-2

The sandwich formed by the thin electrolyte membrane and the two thin electrodes comprises a compact unit on which heat and mass balances may be taken. Hereafter in this section, this "sandwich" will be referred to as the matrix. (a)

The screen in the gas space touches the electrode and distributor at points which are but a small percent of their total surfaces. The screen will, however, increase the effective heat transfer area of these surfaces in the same manner as a fin or other extended surface. The heat and mass transfer coefficients will be increased by the continual mixing action of the screen. It is assumed that all effects of the screen in the gas space can be accounted for by suitable choice of the transfer coefficients.

It is further assumed that the gasket material which separates the cells is a poor conductor of heat and thus that the matrix and distributor plates are insulated at the edges $y = \pm b$ for all values of x . It will be shown that the heat conduction terms will be small compared with the other heat transfer terms so that this assumption will be justified. Concentration gradients through the thickness of the matrix will be neglected: that is, although such a gradient probably does exist, this analysis will concern only the concentration on the hydrogen side which affects the vapor pressure of the water evaporating into the hydrogen stream. The above assumptions greatly aid in the solution of the performance equations because they result in a problem which is one-dimensional.

The assumptions are summarized in the following table:

1. Hydrogen enters uniformly along the center line and leaves uniformly at the edges.
2. The matrix, consisting of the two electrodes and the electrolyte membrane, can be treated as a single unit.

(a) Elsewhere in this report "matrix" refers to the electrolyte membrane only.

3. The effects of the screen in the gas space can be accounted for by suitable mass and heat transfer coefficients.
4. The matrix is insulated against mass and heat transfer at all boundaries.
5. Concentration and temperature gradients through the thickness of the matrix are neglected.
6. The distributor plate is insulated along $y = \pm b$. Thus, there are no gradients normal to the direction of flow.
7. The cell is one of a stack comprising a battery.

6.3.1.2 Derivation of the Performance Equations

The six differential equations which describe the temperature and concentration profiles in the fuel cell were obtained by making energy and mass balances on differential elements across the cell and perpendicular to the direction of hydrogen flow. Energy balances were written for the matrix, the hydrogen stream, and the distributor plate. Mass balances were written for the hydrogen stream, the water in the hydrogen stream and the water in the matrix. These statements are summarized in the following table which also shows the equation numbering system which will be used in the subsequent derivations.

Energy Balances

Mass Balances

	<u>Hydrogen</u>	<u>Water</u>
Matrix (Equation 1)	--	Matrix (Equation 2)
Hydrogen stream (Equation 3)	Hydrogen stream (Equation 4)	Hydrogen stream (Equation 5)
Distributor plate (Equation 6)	--	--

1. Energy balance on the matrix.

It will be recalled that the matrix refers to the "sandwich" composed of the hydrogen electrode, the membrane filled with electrolyte, and the oxygen electrode. Consider a volume element of this matrix which is t centimeter thick, one centimeter wide in the y direction, and of length Δx . The heat entering this volume element is given by

$$-k_m \left. \frac{dT_m}{dx} \right|_x + G_R (I) \cdot \Delta x + c_h(T_h - R)If + c_o(T_o - R)I \frac{f}{2} - c_w(T_m - R)If$$

The first term represents heat in by conduction. The second is the irreversible heat of the reaction. This term depends on the current density, I ma/cm², directly in that this sets the rate of reaction and indirectly since the irreversibility is measured by the difference between open cell voltage and the actual cell voltage. The latter is read from a polarization curve which is a function of the operating conditions, particularly current density. R is a reference temperature for the heat of reaction, and the last three terms represent the heat required to heat the hydrogen and oxygen up to this temperature and then leave the liquid water product at the temperature of the matrix. The factor f converts current density to gram moles per hour per square centimeter.

The heat leaving this volume element is given by

$$-k_m \left. \frac{dT_m}{dx} \right|_{x + \Delta x} + h_2 \Delta x (T_m - T_h) + h_3 \Delta x (T_m - T_o) + k_2 \cdot \Delta x \left[P(N, T_m) - P_{wh} \right] \left[\Delta H_v + c_w (T_m - T_h) \right]$$

The first term is the conduction out at $x + \Delta x$. The second and third terms are convective losses to the hydrogen and oxygen streams. Since the oxygen is dead-ended and the stoichiometric required oxygen is very small this latter term will be small compared to the convective losses to the hydrogen stream. Since we are first considering cases with hydrogen flows several times stoichiometric, we will neglect the oxygen convective term for the present. The last term represents the heat lost by vaporizing the water in the matrix at point x and transferring it into the hydrogen stream at T_h and partial pressure of water P_{wh} . $P(N, T_m)$ is the vapor pressure of water at the matrix temperature T_m and over a KOH solution of normality N . Since the oxygen is dead-ended, there is no vaporization on that side of the matrix.

Since we are looking for a steady state solution, the accumulation of heat in this volume element must be zero. Setting the heat out equal to the heat in, dividing by Δx , and taking the limit as Δx goes to zero gives the first differential or performance equation

$$k_m \frac{d^2 T_m}{dx^2} = G_R(I) + c_h(T_h - R)I^f + c_o(T_o - R)I_2^f - c_w(T_m - R)I^f - h_2(T_m - T_h) - h_3(T_m - T_o) - k_2 \Delta H_v [P(N, T_m) - P_{wh}]. \quad (1-1)$$

The heat of reaction varies slightly with temperature over the range of temperature in a particular battery. Thus, if we take the reference temperature equal to the local matrix temperature, the only approximation involved is that of using a heat of reaction based on an average matrix temperature. Accordingly, our equation becomes

$$k_m \frac{d^2 T_m}{dx^2} = G_m(I) - (c_h I^f + h_2)(T_m - T_h) - (c_o I_2^f + h_3)(T_m - T_o) - k_2 [P(N, T_m) - P_{wh}] [\Delta H_v + c_w(T_m - T_h)] \quad (1-2)$$

This equation can be simplified by considering the magnitude of a few of the terms. The heat capacity of hydrogen or oxygen is about 7 cal/g-mole °C. Current densities have been measured up to 1400 ma/cm², but the usual operating range will probably be less than 500 ma/cm². The hydrogen consumed is

$$3600 \frac{\text{sec}}{\text{hr}} \cdot \frac{1\text{-g-equivalent}}{96494 \text{ amp}\cdot\text{sec}} \cdot \frac{1 \text{ g-mole}}{2 \text{ g-equivalent}} \frac{1 \text{ amp}}{1000 \text{ ma}} I \frac{\text{ma}}{\text{cm}^2}$$

$$= 1.865 \times 10^{-5} I \frac{\text{g-mole}}{\text{hr}\cdot\text{cm}^2},$$

thus the conversion factor

$$f = 1.865 \times 10^{-5} \frac{\text{g-mole}}{\text{hr}\cdot\text{ma}}$$

and the quantity

$$cIf = 7 \times 1400 \times 1.865 \times 10^{-5} = 0.18 \frac{\text{cal}}{\text{hr}\cdot\text{cm}^2\text{°C}}$$

as a maximum. For laminar flow between parallel plates the quantity

$$hD_e/k \approx 8 \quad (1-3)$$

The equivalent diameter for parallel plates is twice the spacing or 0.4 centimeters maximum. For hydrogen, $k = 1.82 \text{ cal/hr}\cdot\text{cm}^2\text{°C}$, so that

$$h_{\min} = 8 \frac{1.82}{0.4} = 36 \frac{\text{cal}}{\text{hr}\cdot\text{cm}^2\text{°C}} \quad (1-4)$$

or

$$h \gg cIf. \quad (1-5)$$

In addition, the sensible heat required to raise the vaporized water from the matrix temperature to the stream temperature is small compared with the latent heat, that is

$$\Delta H_v \gg c_w(T_m - T_h) \quad (1-6)$$

since $T_m - T_h$ will certainly be less than ten degrees. Inequalities (1-5) and (1-6) state that the sensible heat terms involving reactants and product going between the stream and matrix temperatures are negligible.

The performance equation becomes:

$$k_m \frac{d^2 T_m}{dx^2} = G_m(I) - h_2(T_m - T_h) - k_2 \Delta H_v [P(N, T_m) - P_{wh}] \quad (1-7)$$

The cell is **symmetric** at $x = 0$ and the matrix is clamped in place with gaskets so that it is essentially insulated at $x = a$. Thus we have the boundary conditions

$$\frac{dT_m}{dx} = 0 \quad x = \begin{cases} 0 \\ a \end{cases} \quad (1-8)$$

2. Water balance in the matrix

Let N_w be the flux of water in the matrix in the x-direction, g-moles/hr·cm². Then, considering the same matrix volume element, the water formed is fI and the total entering is given by

$$N_w t \Big|_x + fI \Delta x$$

The water leaving is

$$N_w t \Big|_{x + \Delta x} + k_2 \cdot \Delta x [P(N, T_m) - P_{wh}]$$

Again, setting these two expressions equal, dividing by Δx , and taking the limit as Δx goes to zero gives the second performance equation

$$t \frac{dN_w}{dx} = fI - k_2 [P(N, T_m) - P_{wh}] \quad (2-1)$$

Now,

$$N_w = - D_w \frac{dX_w}{dx} + X_w (N_w + N_{KOH}) \quad (2-2)$$

where

ϕ = total molal concentration of electrolyte

D_w = diffusivity of water in the matrix

X_w = mole fraction water in electrolyte

At steady state, the molar flux of KOH, N_{KOH} will equal zero. Thus,

$$N_w = - \frac{\phi D_w}{1 - X_w} \cdot \frac{dX_w}{dx}, \quad (2-3)$$

and the performance equation becomes

$$\frac{\phi D_w}{1 - X_w} \left[\frac{d^2 X_w}{dx^2} - \frac{1}{1 - X_w} \frac{dX_w}{dx} \right] = fI - k_2 \left[P(N, T_m) - P_{wh} \right] \quad (2-4)$$

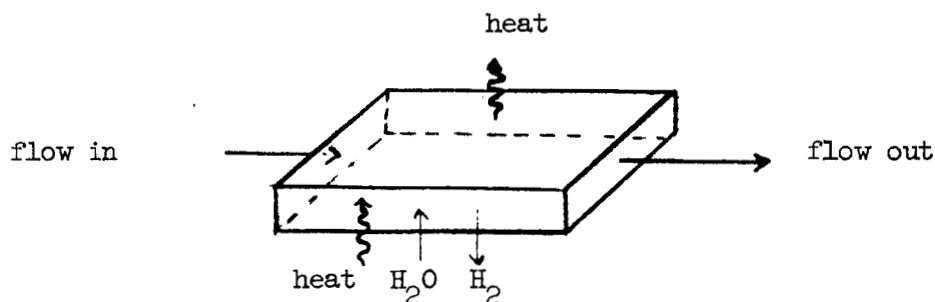
with boundary conditions

$$\frac{dX_w}{dx} = 0 \quad \text{at } x = \begin{cases} 0 \\ a \end{cases}, \quad (2-5)$$

since the matrix is insulated at the edges and the cell is **symmetric**.

3. Energy balance on the hydrogen stream.

Consider next an element of the hydrogen stream of unit width and of length Δx flowing between the distributor plate and the electrode or matrix surface.



The enthalpy in is given by

$$(W_h H_h + W_{wh} H_w) \Big|_x + h_2 \Delta x (T_m - T_h) + k_2 \Delta x [P(N, T_m) - P_{wh}] H_w,$$

where the terms represent the enthalpy in with the flowing stream, the convective transfer from the matrix, and the enthalpy associated with the water evaporating into the stream, respectively. The enthalpy out is

$$(W_h H_h + W_{wh} H_w) \Big|_{x+\Delta x} + \Delta x + h_1 \Delta x (T_h - T_d) + fI \cdot \Delta x \cdot H_h,$$

where the terms represent the enthalpy out with the flowing stream, the convective transfer to the distributor, and the enthalpy out with the reacting hydrogen. Equating these two expressions, dividing by Δx and letting Δx approach zero gives

$$\begin{aligned} \frac{d(W_h H_h + W_{wh} H_w)}{dx} &= h_2 (T_m - T_h) - h_1 (T_h - T_d) \\ &+ k_2 [P(N, T_m) - P_{wh}] H_w - fI H_h \end{aligned} \quad (3-1)$$

Differentiating the left side gives

$$W_h \frac{dH_h}{dx} + W_{wh} \frac{dH_{wh}}{dx} + H_h \frac{dW_h}{dx} + H_w \frac{dW_{wh}}{dx}.$$

Now,

$$\frac{dH}{dx} = \frac{dH}{dT} \cdot \frac{dT}{dx} = c \frac{dT}{dx} \quad (3-2)$$

and from the hydrogen and water balances on the hydrogen stream

$$\frac{dW_h}{dx} = -fI \quad (4-2)$$

$$\frac{dW_{wh}}{dx} = k_2 [P(N, T_m) - P_{wh}]. \quad (5-1)$$

Thus the performance equation becomes simply

$$(W_h c_h + W_{wh} c_w) \frac{dT_h}{dx} = h_2(T_m - T_h) - h_1(T_h - T_d) \quad (3-3)$$

The inlet hydrogen stream temperature will be known so that the boundary condition is

$$T_h = T_h(\text{in}) \text{ at } x = 0 \quad (3-4)$$

4. Mass balance on the hydrogen stream.

The flow rate of hydrogen per unit width, W_h g-moles/hr·cm, decreases in the direction of flow as the hydrogen is consumed in the electrode reaction. Referring to the same unit volume used in the previous section, a steady-state hydrogen balance may be written

$$W_h \Big|_x = W_h \Big|_{x + \Delta x} + fI \cdot \Delta x \quad (4-1)$$

or

$$\frac{dW_h}{dx} = -fI, \quad (4-2)$$

with the boundary condition

$$W_h = W_h(\text{in}) \text{ at } x = 0. \quad (4-3)$$

The solution to this equation is simply

$$W_h = W_h(\text{in}) - fIx. \quad (4-4)$$

If we define the flow rate in terms of the parameter

$$F = \frac{\text{hydrogen fed to the cell}}{\text{hydrogen consumed in the reaction}}, \quad (4-5)$$

then the solution becomes

$$W_h = fI(aF - X), \quad (4-6)$$

where a is the length of the cell in the direction of flow. The change in flow rate across the cell becomes negligible for the case when all cooling is done by excess hydrogen flow.

5. Water balance on the hydrogen stream.

The product water from the cell reaction is removed by evaporation into the hydrogen stream. The flow rate of water in this stream, W_{wh} g-moles/hr·cm, increases with x . Considering the same volume element, a water balance gives

$$W_{wh} \Big|_{x + \Delta x} = W_{wh} \Big|_x + k_2 \Delta x \left[P(N, T_m) - P_{wh} \right],$$

which yields the differential equation

$$\frac{dW_{wh}}{dx} = k_2 \left[P(N, T_m) - P_{wh} \right]. \quad (5-1)$$

This is a nonlinear equation since the partial pressure of water in the hydrogen stream, P_{wh} , is a function of the water and hydrogen flow rates and the total pressure, π , i.e.,

$$P_{wh} = \frac{W_{wh}}{W_h + W_{wh}} \pi. \quad (5-2)$$

The partial pressure of water in the inlet stream will be known so that the boundary condition for equation (5-1) is

$$W_{wh} = W_{wh}(\text{in}) \quad \text{at } x = 0 \quad (5-3)$$

6. Energy balance on the distributor plate.

Heat can be transferred to the distributor plate from both the hydrogen and oxygen streams. If coolant is being pumped through channels in the distributor plate, there will be transfer to this stream also. This will apply only to those points along x where coolant is flowing. To denote these areas let the function $S(x)$ be defined such that

$$S(x) = \begin{cases} 0 & \text{if there is no coolant flowing at } x \\ 1 & \text{if there is coolant flowing at } x. \end{cases} \quad (6-1)$$

Let l be the distributor thickness and k_d be an effective thermal conductivity in the x direction. Then the heat input to a volume element of unit width, l thickness, and Δx length is given by:

$$- k_d l \left. \frac{dT_d}{dx} \right|_x + h_l \Delta x (T_h - T_d) + h_u \Delta x (T_o - T_d).$$

The heat out is given by

$$- k_d l \left. \frac{dT_d}{dx} \right|_{x + \Delta x} + S(x) h_c \Delta x (T_d - T_c)$$

This leads to the performance equation

$$k_d l \frac{d^2 T_d}{dx^2} = h_l (T_d - T_h) + h_u (T_d - T_o) + S(x) h_c (T_d - T_c) \quad (6-2)$$

There is a restriction on this equation and therefore also on the hydrogen stream equations which must be mentioned at this point. If the coolant which is flowing in the distributor is too cold it will cause the water in the hydrogen stream to condense. This must be avoided from an operational viewpoint, so we introduce the restriction

$$T_d > T_h(\text{sat}), \quad (6-3)$$

where $T_h(\text{sat})$ is the dew point of the hydrogen stream.

Since the hydrogen enters from a channel in the distributor at $x = 0$, a reasonable estimate for the initial condition on T_d is

$$T_d(0) = T_h(\text{in}) \quad \text{at } x = 0 \quad (6-4)$$

The boundary condition at $x = a$ will depend on the final design. For some type of fin extended from the distributor or for a coolant in a channel along the edge, the end condition might read

$$T_d = T_d(a) \quad \text{at } x = a. \quad (6-5)$$

For the cases of gas cooling alone or gas cooling with internal coolant channels the end condition becomes

$$\frac{dT_d}{dx} = 0 \quad \text{at } x = a \quad (6-6)$$

6.3.2 Solution for the Dynamic System with No Auxiliary Cooling

For this case, the flow rate of hydrogen can be from twenty to one hundred-fifty times the stoichiometric requirement. The heat transfer terms on the oxygen side may be safely neglected. In addition, there is no coolant flowing in the distributor plates so that these terms in the performance equation (6-2) are deleted.

The performance equations developed in the preceding section lend themselves to considerable simplification. As a first approximation to the solution, all the diffusion terms were neglected. This leads to the linear solution described in the next section. These approximations are not as severe as it first appears. The cross sectional area available for diffusion of heat and mass in the matrix is very small. The thickness of this unit is only about 0.06 inches. In its present state of development, the distributor plate is conceived to be of thin sheet metal with comparatively large gas spaces. Thus, its effective thermal conductivity in the x-direction is quite low. An analog computer was used to solve the complete performance equations. The results of this simulation verify the assumptions of negligible water diffusion in the matrix and negligible heat conduction in the distributor plate, and show that the linear solution can correctly be used in the design of a gas dried-gas cooled fuel cell system.

6.3.2.1 Linear Solution

For this solution it is assumed that the diffusion of water and heat in the matrix and the conduction of heat in the distributor plate are negligible. The performance equations become

$$G_m = h_2(T_m - T_h) + \Delta H_v fI \quad (1-9)$$

$$fI = k_2 \left[P(N, T_m) - \frac{W_{wh}}{W_h + W_{wh}} \pi \right] \quad (2-6)$$

$$\frac{dT_h}{dx} = \frac{h_2(T_m - T_h) - h_1(T_h - T_d)}{W_h c_h + W_{wh} c_w} \quad (3-3)$$

$$T_h = T_h(in) \text{ at } x = 0 \quad (3-4)$$

$$W_h = W_h(in) - fIx \quad (4-4)$$

$$\frac{dW_{wh}}{dx} = k_2 \left[P(N, T_m) - P_{wh} \right] \quad (5-1)$$

$$W_{wh} = W_{wh}(in) \text{ @ } x = 0 \quad (5-3)$$

$$0 = h_1(T_d - T_h) \quad (6-2)$$

Combining (5-1) and (2-6) gives

$$\frac{dW_{wh}}{dx} = fI \quad (7-1)$$

and solving, using (5-3),

$$W_{wh} = W_{wh}(in) + fIx. \quad (7-2)$$

Combining (1-9), (3-3) and (6-2) yields

$$\frac{dT_h}{dx} = \frac{G_m - \Delta H_v fI}{W_h c_h + W_{wh} c_w} \quad (7-3)$$

and using the results (4-4) and (7-2)

$$\frac{dT_h}{dx} = \frac{G_m - \Delta H_v fI}{[W_h(in) c_h + W_{wh}(in) c_w] + fI(c_w - c_h)x}. \quad (7-4)$$

This equation can be solved, but a further simplification is possible.

For gas cooling, the hydrogen rate is at least twenty times stoichiometric, i.e.,

$$W_h(in) > 20a(fI).$$

In order to avoid drying the membrane a high water content of the hydrogen stream is maintained so that W_{wh} is usually greater than twenty percent of W_h . In addition, $c_w = 8.1 \text{ cal/g-mole}^\circ\text{C}$ and $c_h = 6.95$ but $(c_w - c_h) = 1.15$ so that in the range of x under consideration,

$$\left[W_h(\text{in})c_h + W_{wh}(\text{in})c_w \right] \gg fI(c_w - c_h)x . \quad (7-5)$$

Thus, the solution to equation (7-4) is simply

$$T_h = T_h(\text{in}) + \frac{G_m - \Delta H_v fI}{W_h(\text{in})c_h + W_{wh}(\text{in})c_w} x . \quad (7-6)$$

The temperature of the matrix is found by solving Equation (1-9) to give

$$T_m = T_h + \frac{G_m - \Delta H_v fI}{h_2} . \quad (7-7)$$

The vapor pressure of water over the matrix, $P(N, T_m)$, is given by a polynomial in N times the vapor pressure of pure water at T_m (Ref. 1).

$$P(N, T_m) = P_N \cdot P_o(T_m) \quad (7-8)$$

$$= \left\{ \begin{array}{ll} 1 - 0.0350N - 0.003415N^2, & N < 6 \\ 1.1836 - 0.0962N + 0.001685N^2, & N > 6 \end{array} \right\} P_o(T_m) . \quad (7-9)$$

A curve of P_N versus N is given in Figure 3. Solution of (2-6) for $P(N, T_m)$ gives

$$P(N, T_m) = \left(\frac{W_{wh}}{W_{wh} + W_h} \right) \pi + \frac{fI}{k_2} .$$

So the quantity

$$P_N = \frac{\left(\frac{W_{wh}}{W_{wh} + W_h} \right) \pi + \frac{fI}{k_2}}{P_o(T_m)} ,$$

can be computed for any point x and then N can be determined by reference to Figure 3.

VAPOR PRESSURE DATA CORRELATION

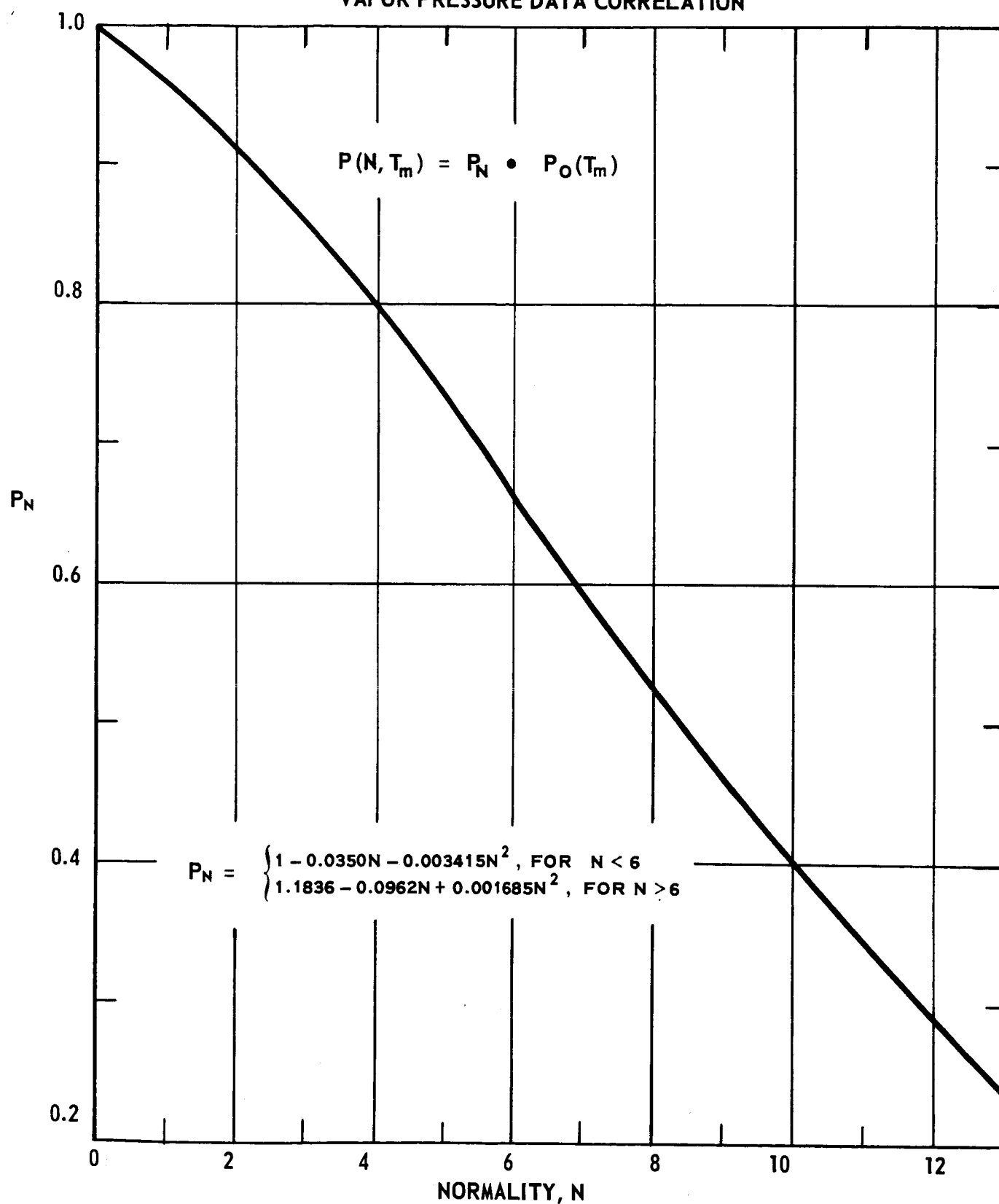


FIGURE 6-3

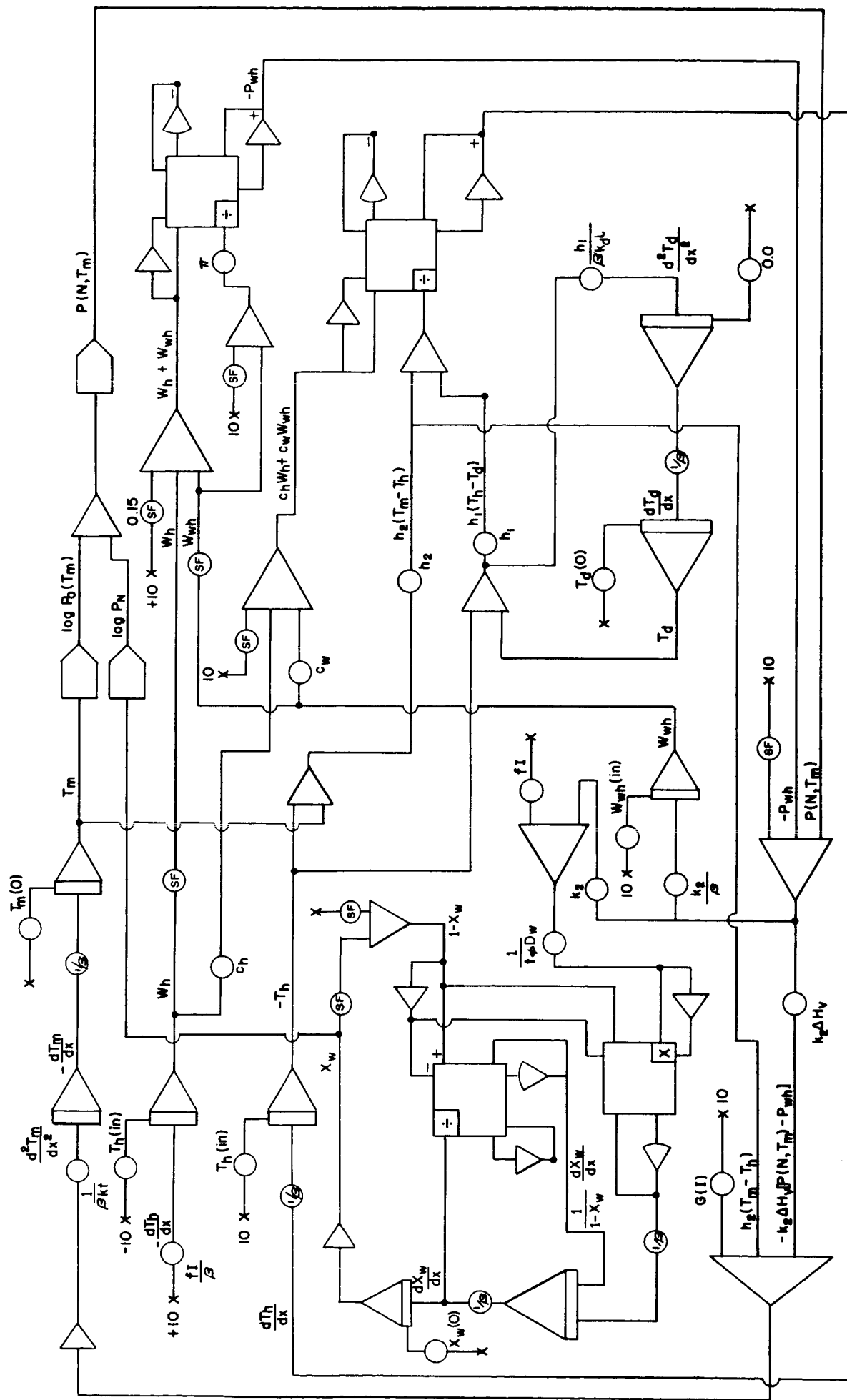
6.3.2.2 Analog Solution

To obtain an actual solution, the set of differential performance equations was programmed for an analog computer. The diagram for the circuit, with the variables written in unscaled form, is shown in Figure 6-4. The results of this solution verified that the diffusion of water in the matrix and diffusion of heat in the distributor plate were completely negligible. The effect of heat conduction in the matrix was slight. Temperature profiles given by the analog began with a zero slope (dictated by the boundary conditions), but quickly became linear. The temperature of the distributor was equal to the temperature of the hydrogen stream and the temperature difference between the matrix and hydrogen was the same as in the linear solution. For the case of gas-cooling gas-drying, the temperature and concentration profiles are monotonic, with their extreme values at the end conditions. These values are the same in both solutions. The differences in the actual profile are small and it is concluded that the linear solution may be correctly used in design of this fuel cell system.

6.3.3 Application to Dynamic System with No Auxiliary Cooling

A typical fuel cell system showing hydrogen, oxygen and coolant streams is shown in Figure 6-5. Five parameters must now be given to determine the system. Assume that the desired operating pressure is 4 atmospheres, the current density is 450 ma/cm² and the cell voltage is 0.8 volts. Table 6-2 shows the normality ranges for ten different cases under the above conditions.

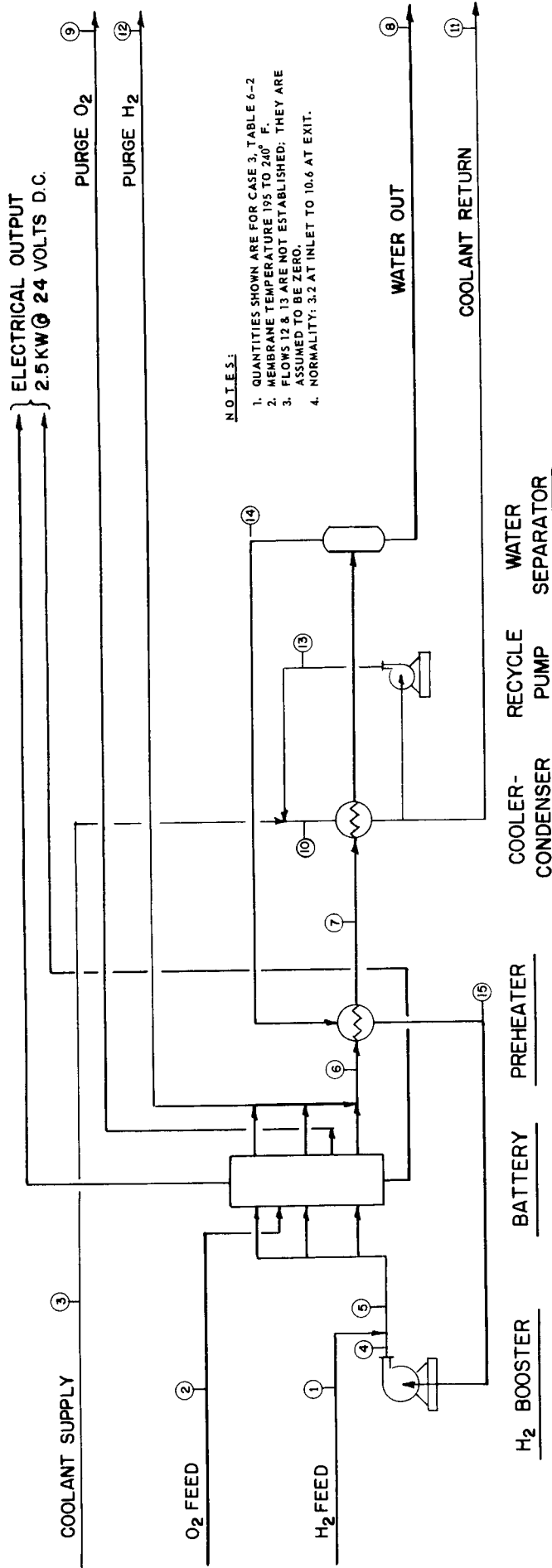
ANALOG SIMULATION OF A HYDROGEN-OXYGEN FUEL CELL (STEADY STATE)



NOTE ; SCALE FACTORS OTHER THAN β ARE NOT SHOWN. POTENTIOMETERS MARKED SF FURNISH THESE SCALE FACTORS

FIGURE 6-4

PRELIMINARY FLOW SHEET
DYNAMIC SYSTEM WITH NO AUXILIARY COOLING



NOTES:

1. QUANTITIES SHOWN ARE FOR CASE 3, TABLE 6-2
2. MEMBRANE TEMPERATURE 195 TO 240° F.
3. FLOWS 12 & 13 ARE NOT ESTABLISHED; THEY ARE ASSUMED TO BE ZERO.
4. NORMALITY: 3.2 AT INLET TO 10.6 AT EXIT.

STREAM	1	2	3	4	5	6	7	8	9	10	11	12	13	14	15
HOURLY FLOWS															
H ₂	0.26	0.13	—	—	—	—	—	—	—	—	—	—	—	—	—
O ₂	—	—	—	—	—	—	—	—	—	—	—	—	—	—	—
Ar	—	2.165	0.0677	—	—	—	—	—	0.086	0.0027	—	—	—	—	—
H ₂ O	—	0.012	0.0003	—	—	—	—	—	0.012	0.0003	—	—	—	—	—
ETG	—	—	—	—	—	—	—	—	0.009	0.0005	—	—	—	—	—
TOTAL	0.26	0.13	—	—	—	—	—	—	0.107	0.0035	—	—	—	—	—
PSIA	58.8	58.8	75	58.8	58.8	57.8	57.6	56.3	57.8	65	65	—	—	56.3	56.1
°F.	90.0	90.0	140.0	194.0	194.0	239.4	232.7	187.3	220	160.0	160.0	—	—	187.3	194.0
STATE	V	V	L	V	V	V	V	L	V	L	L	—	—	V	V

FIGURE 6-5

TABLE 6-2

Concentration Gradients as a Function of Inlet Flow Conditions

<u>Case Number</u>	<u>F</u>	<u>H₂ leaving condenser T_{h_c} °C.</u>	<u>Maximum matrix temp T_{m_{out}} °C.</u>	<u>Preheat ΔT_p</u>	<u>N_{in}</u>	<u>N_{out}</u>
1	137	86.3	104.5	0	0.5	7.9
2	137	86.3	108.3	3.7	3.2	9.1
3	100	86.3	115.7	3.7	3.2	10.6
4	65	86.3	129.3	3.7	3.2	15
5	137	70.9	100	10.4	6.4	11
6	137	75.0	100	4.9	3.9	10
7	110	75.0	105	4.9	3.9	11.2
8	78	75.0	115	4.9	3.9	12.8
9	55	75.0	130	4.9	3.9	15
10	47	75.0	138	4.9	3.9	17

I = 450 ma/cm²

E = 0.80 volts

π = 4 atm

F = H₂ flow rate/stoichiometric H₂ requirementT_{h_c} = Temperature H₂ leaving the condenserΔT_p = Temperature rise across the preheaterN_{in} = normality of entrance pointN_{out} = normality at exit pointT_{m_{out}} = Temperature of matrix at outlet (maximum matrix temperature)

Consider first the system without preheater, i.e., in Figure 6-5 let the area of the preheater equal zero. The choice of the condenser outlet temperature then sets the inlet normality at 0.5. Reference to equations (7-7) and (7-11) shows that without a preheat of the incoming hydrogen the normality of the membrane near the entrance will always be low. According to Equation (7-7) the difference between the matrix and hydrogen temperatures will be

$$T_m - T_h = \frac{G_m - H_v f I}{h_2} .$$

The difference between the equilibrium vapor pressure of water over the electrolyte and that of the water in the hydrogen stream is

$$P(N, T_m) - P_{wh} = \frac{f I}{k_2} .$$

The numerators of the fractions on the right side of these two equations are small and an accurate value of the transfer coefficients is not necessary. A discussion of the effects of these values, including the maximum and minimum cases, is given in Appendix B. For the case under discussion here, the temperature difference is about one degree Centigrade and the difference

in partial pressures is about 0.05 psia. Since P_{wh} for this case is 7.85 psia, the value of $P(N, T_m)$ is very close to P_{wh} . However, P_{wh} was set by the condenser as the vapor pressure of water, $P_o(T)$, at the condenser temperature 86.3. This is only about one degree lower than the inlet matrix temperature. Thus, if the water formed there is to be evaporated, the electrolyte vapor pressure, $P(N, T_m)$, must be high enough to transfer water to the stream at P_{wh} . Since

$$P(N, T_m) = P_N \cdot P_o(T_m)$$

and $P_o(T_m)$ is only slightly higher than P_{wh} , P_N must be close to unity. If the hydrogen stream is preheated slightly the value of $P_o(T_m)$ increases and the inlet normality rises. A convenient source of this preheat is the outlet hydrogen stream. Accordingly, all the remaining cases given in Table 6-2 include a hydrogen preheater.

The remaining cases in Table 6-2 show the effect of condenser temperature and hydrogen flow rate. A lower condenser temperature, which has the disadvantage of requiring extra area, allows operation at a lower cell temperature for a given flow rate (compare cases 2 and 6) or at a lower flow rate for a given maximum cell temperature (compare cases 3 and 8). At a given condenser temperature, decreasing the flow rate increases the maximum cell temperature and the concentration gradient across the cell (cases 6-10).

The fifth column, ΔT_p , shows that the average normality of the entire cell may be increased by increasing the amount of preheat.

The shape of the normality profiles for two cases with the following conditions:

π	= total pressure	= 1 atm
I	= current density	= 100 ma/cm ²
T _c	= condenser outlet	= 60°C
T _{out}	= outlet H ₂ temperature	= 88°C no preheat = 91°C with preheat
F	= H ₂ flow ratio	= 75

is shown in Figure 6-6. In the first case, there is no preheat and in the second the hydrogen stream is preheated three degrees.

TYPICAL NORMALITY PROFILE
DYNAMIC SYSTEM WITH NO AUXILIARY COOLING

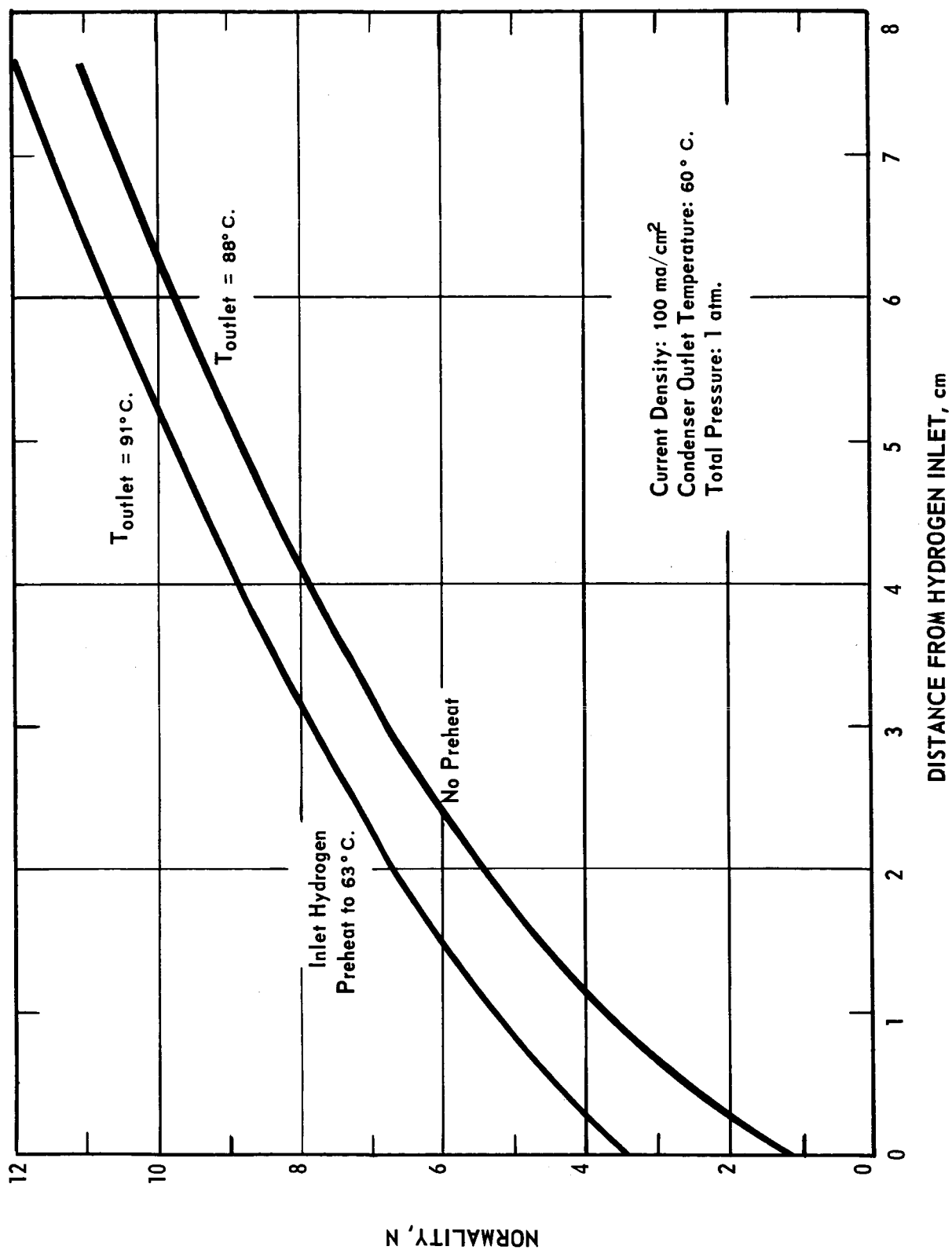


FIGURE 6-6

6.3.4. Summary - Dynamic System with No Auxiliary Cooling

The simulation predicts that for dynamic heat and water removal with no auxiliary cooling:

1. The temperature and partial pressure of water in the bulk hydrogen stream will be essentially the same as at the adjacent electrode surface at any point in the cell at current densities at least as high as 450 ma/cm².
2. At the high hydrogen recycle rate required for the dynamic system with no auxiliary cooling, the change in the water content of the hydrogen stream as it passes through the cell is very small. Consequently, for a given water content in the hydrogen entering the cell, the steady state electrolyte concentration gradient over the face of the electrode will depend only on the temperature gradient.
3. The temperature and electrolyte concentration gradients should be independent of the number of inlet hydrogen channels, and consequently, should be independent of the distance between the inlet and outlet channels, at least down to distances at which the diffusion of heat and/or water within the matrix becomes significant. While additional calculation estimating this distance remains to be made, work already performed on the analog computer indicates that it is less than 1-1/2 inches. Should calculation show that the interchannel distance required to even out temperature and electrolyte concentration gradients is too small for reasonable cell construction, there would be no advantage in providing more than one inlet and one or two outlet channels for the recycle hydrogen.

4. Preheating of the hydrogen stream entering the battery, preferably by the exit hydrogen stream, would be required to maintain the KOH concentration above 3-5N at the gas inlet. (This would be necessary since, as shown in Section 5, cell performance declines sharply at KOH concentration below 3-5N, particularly at current densities above 100 ma/cm².)

5. In a dynamic system with no auxiliary cooling, maintenance of the electrolyte loading within the limits defined in Section 5, e.g., 2.0-3.0 g/g for ACCO Asbestos, may be difficult, since these loading limits set limits of 2-3N variation in electrolyte concentration, regardless of what electrolyte concentration initially is put in the matrix. On the other hand, provision of auxiliary internal cooling should simplify the problem of limiting the variation in electrolyte concentration to within 2-3N, by minimizing the temperature gradient. This, then, is an additional advantage of the dynamic system with auxiliary cooling. In the Second Quarterly Report,⁽²⁾ it was shown that a dynamic system with auxiliary cooling would be more desirable than one without auxiliary cooling because the former would require a considerably smaller hydrogen recycle rate, resulting in a recycle pump weighing less and consuming less parasitic power.

7. FUTURE WORK

During the fourth quarterly period, work on Phase I of the Work Schedule will continue in the following areas:

(a) Develop techniques for protecting or suitable materials for replacing nickel electrode support screens. The use of precious metal plating, inert plastic materials, or more resistant alloys will be studied.

(b) Investigate further the effect of pressure on cell performance, and the inter-relationships between pressure and other operating variables such as temperature and electrolyte concentration.

(c) Extend the study of operating variables to include temperatures up to at least 150°C, and electrolyte concentrations up to the limits imposed by solubility.

(d) Continue life-testing to study operation at higher temperatures (to 100°C), higher current densities (200-400 ma/cm²), and pressures above atmospheric. Improved electrode support materials will also be evaluated.

In the third quarter, work on Phase II was initiated. This work will be continued in the following areas:

(a) The 6 inch x 6 inch cell will be evaluated in operational tests over a range of operating conditions and test durations.

(b) Analysis of heat and mass transfer problems associated with battery operation will continue. In particular, the use of an internal coolant for heat removal will be studied.

(c) Design of a 2 kilowatt battery, using bipolar separator plates of novel construction, will be completed. The design will emphasize light-weight construction, and will be based on the studies of the effect of operating variables and the analysis of heat and mass transfer problems described in the preceding paragraphs.

APPENDIX A

Nomenclature for Mathematical Analysis

Symbol	Definition	Units
a	one-half electrode length in x-direction	cm
b	one-half electrode length in y-direction	cm
c_j	heat capacity of j	cal/g-mole ^o C
D_w	diffusivity of water in matrix	cm ² /hr
D_k	diffusivity of K ⁺ ions in matrix	cm ² /hr
f	moles H ₂ consumed per hr. per ma of current	g-moles/hr.ma
F	moles H ₂ fed/mole H ₂ reacted	
$G_R(I)$	heat generated due to irreversibility with reactants entering at R ^o C and the product being liquid water at R ^o C.	cal/hr.cm ²
$H_j(T)$	enthalpy of component j at temperature T	cal/g-mole
h_1	heat transfer coefficient at hydrogen distributor plate	cal/hr.cm ² °C
h_2	heat transfer coefficient at hydrogen electrode	cal/hr.cm ² °C
h_3	heat transfer coefficient at oxygen electrode	cal/hr.cm ² °C
h_4	heat transfer coefficient at oxygen distributor plate	cal/hr.cm ² °C
I	Current density	ma/cm ²
k_2	mass transfer coefficient at hydrogen electrode	g-moles/hr.cm ² psig
K_1	conversion factor	cal/hr.watt
k_d	effective thermal conductivity of the distributor plate	cal/hr.cm ² °C/cm
k_m	effective thermal conductivity of matrix composed of screen-electrode-solution and membrane-electrode-screen	cal/hr.cm ² °C/cm
l	thickness of distributor plate	cm
N	normality of KOH solution in matrix	equiv/liter
N_w	mass flux of water	g-moles/cm ² hr
$P(N,T)$	partial pressure of water over matrix at temperature T and normality N	psia
P_{wj}	partial pressure of water in j stream j=h=hydrogen j=o=oxygen	psia
R	reference temperature	°C

<u>Symbol</u>	<u>Definition</u>	<u>Units</u>
t	thickness of membrane + electrodes	cm
T	temperature	°C
w _j	flow rate of j	g-moles/hr·cm of width
x	distance coordinate	cm
y	distance coordinate	cm
ϕ	molar concentration of "density"	g-moles/cm ³
π	total pressure	psia

Subscripts

h	hydrogen
o	oxygen
w	water
m	matrix
d	distributor
c	coolant
wh	water in the H ₂ stream

APPENDIX B

Effect of Transfer Coefficients

In the preceding discussion, it was noted that the lack of accurate values of the transfer coefficients did not seriously affect the results. This assumption will be most severe for the case of high current density when the numerators in equations (7-7) and (7-10) are greatest. Consider then case 8 in Table 6-2 in which $I = 450 \text{ ma/cm}^2$. The inlet normality for this case was 3.9 and the outlet 12.8.

The maximum value for k_2 may be taken as infinity. The minimum value would correspond to pure molecular diffusion across the width of the channel, δ . This gives

$$k_2 \text{ min} = \frac{D_{wh}}{R\delta T} = 0.093 \frac{\text{g-moles}}{\text{hr}\cdot\text{cm}^2\cdot\text{psia}}$$

The k_2 value used in these calculations was 0.2. The values below show the small effect of not actually knowing k_2 , including the extreme case of $k_2 = 0.1 k_2 \text{ min}$

k_2	N_{in}	N_{out}
∞	4.05	12.9
0.2	3.9	12.8
0.093	3.8	12.8
0.009	2.1	12.2

For the heat transfer coefficient we may again take the maximum value as infinity. For the minimum value, let us assume that the hydrogen is in laminar flow between the parallel plates of the electrode and distributor, but neglect the mixing effect of the screen and its addition to the heat transfer area. In addition, assume that the heat is generated not at

the surface of the electrode but at its center and that all the heat must be transferred to the surface through the least conductive material in the electrode, i.e., Teflon. For laminar flow between parallel plates

$$\frac{hD_e}{k} \approx 8$$

or

$$h_{2min} = 8 \cdot \frac{1.82}{0.2} = 73 \frac{\text{cal}}{\text{hr} \cdot \text{cm}^2 \cdot ^\circ\text{C}}$$

Also through half the electrode

$$\Delta T = (q/A) \frac{t/2}{k} = 2.1^\circ\text{C}$$

A value of h_2 of 360 was used, based on the assumption that after each wire in the screen, the hydrogen is mixed and the effect is similar to the heat transfer in the inlet region of a channel. The extended surface of the electrodes furnished by the screens and the turbulence caused by the gas flowing around the screens both will increase the value of h_2 over h_{2min} . The calculated concentration differences resulting from these several values of h_2 are shown below.

	N_{in}	N_{out}
$h_2 = \infty$	3.8	12.8
$h_2 = 360$	3.9	12.8
$h_2 = 76$	4.9	13.1
$h_2 = 76$ plus a 2.1°C rise thru the electrode	5.8	13.4

Thus, using reasonable or even minimum values for the transfer coefficients does not seriously change the results.

References

1. "Research and Development of High-Performance Light-Weight Fuel Cell Electrodes", American Cyanamid Company, First Quarterly Report Nov. 1, 1963 to Jan. 31, 1964, NAS CR-54022.
2. *ibid*, Second Quarterly Report, Feb. 1 to Apr. 30, 1964, NAS CR-54084.
3. M. A. Klechko and M. M. Godneva, Zhur. Neorg. Khim. (Russian) 4, 2130 (1959).
4. A. M. Adams, F. T. Brown, and R. G. H. Watson (1963) in "Fuel Cells" (W. Mitchell, Jr., ed.) p. 138 (Interscience).

DISTRIBUTION LIST FOR SECOND QUARTERLY REPORT

National Aeronautics & Space Administration
Washington, D. C. 20546
Attention: Miss Millie Ruda, Code AFSS-LD 3
Attention: Walter L. Scott, Code RPP 1
Attention: Ernst M. Cohn, Code RPP 1
Attention: George E. Esenwein, Code MSA 1
Attention: H. B. Finger, Code RP 1
Attention: A. M. Andrus, Code FC 1
Attention: J. R. Miles, Code SL 1
Attention: Fred Schulman, Code RN 1

National Aeronautics & Space Administration
Goddard Space Flight Center
Greenbelt, Maryland
Attention: Thomas Hennigan 1

National Aeronautics & Space Administration
Lewis Research Center
21000 Brookpark Road
Cleveland, Ohio 44135
Attention: B. Lubarsky, MS 86-1 1
Attention: N. D. Sanders, MS 302-1 1
Attention: N. T. Musial, MS 77-1 1
Attention: M. J. Sarri, MS 86-1 1
Attention: R. L. Cummings, MS 86-1 1
Attention: H. J. Schwartz, MS 86-1 1
Attention: John E. Dilley, MS 86-1 1
Attention: W. A. Robertson, MS 86-1 1 + 1 repro.

National Aeronautics & Space Administration
Marshall Space Flight Center
Huntsville, Alabama
Attention: Philip Youngblood 1
Attention: Eugene Cagle 1

National Aeronautics & Space Administration
Manned Space Craft Center
Houston 1, Texas
Attention: W. R. Dusenbury 1
Systems Evaluation & Development Div.
Rich Building
6040 Telephone Road
Attention: Robert Cohen 1
Gemini Project Office

National Aeronautics & Space Administration
Scientific and Technical Information Facility
P. O. Box 5700
Bethesda, Maryland
Attention: NASA Representative 2 + 1 repro.